Palaeogeography, Palaeoclimatology, Palaeoecology 303 (2011) 20–37

Contents lists available at ScienceDirect

Palaeogeography, Palaeoclimatology, Palaeoecology

journal homepage: www.elsevier.com/locate/palaeo

Late Quaternary stratigraphic analysis of the Lake Malawi Rift, East Africa: An integration of drill-core and seismic-reflection data

Robert P. Lyons [a,*], Christopher A. Scholz [a], Matthew R. Buoniconti [b], Matthew R. Martin [c]

[a] Department of Earth Sciences, Syracuse University, 204 Heroy Geology Laboratory, Syracuse, NY 13244, USA
[b] Chevron Corporation, 6001 Bollinger Canyon Road, San Ramon, CA 94583, USA
[c] Newfield Exploration Company, 363 North Sam Houston Parkway East, Suite 2020, Houston, TX 77060, USA

ARTICLE INFO

Article history:
Received 1 December 2008
Received in revised form 8 April 2009
Accepted 13 April 2009
Available online 22 April 2009

Keywords:
East Africa
Seismic stratigraphy
Paleoclimatology
Scientific drilling
Lake Malawi

ABSTRACT

Lake Malawi contains a long continuous sedimentary record of climate change in the southern hemisphere African tropics. We develop a stratigraphic framework of this basin over the last ~150 ka by integrating several vintages of seismic-reflection data with recently acquired drill cores. In the seismic-reflection data set, we document three lake-level cycles where progradational delta seismic facies and erosional truncation surfaces mark the basal boundary of each sequence. The clinoform packages and their down-dip, time-equivalent surfaces can be mapped throughout each basin, where each major lowstand surface was followed by a transgression and highstand. On several occasions, lake level dropped as much as 500 m below present lake level (BPLL) in the North Basin and 550 m BPLL in the Central Basin, resulting in a 97% reduction of water volume and 89% reduction of water surface area relative to modern conditions. Evidence for these lake-level fluctuations in the drill cores includes major changes in saturated bulk density, natural gamma ray values, and total organic carbon. During lowstands, density values doubled, while total organic carbon values dropped from ~5% to 0.2%. Coarse-grained sediment and organic matter flux into the basin were higher during transgressions, when precipitation, runoff, sediment supply, and nutrient input were high. This sedimentation pattern is also observed in seismic-reflection profiles, where coarse-grained seismic facies occur at the bases of sequences, and in the drill-core data where the highest total organic carbon values are observed immediately above lowstand surfaces.

1. Introduction

The influence of the tropical continental regions on global heating and moisture transport is poorly understood. Continents disrupt ocean circulation and the position of the Inter-Tropical Convergence Zone (ITCZ), thus playing a crucial role in modulating global climate. In order to understand the continental response to orbitally-induced insolation variability, long continuous continental climate records are needed. Only recently have these records emerged, and with the development of continental lake drilling projects around the world, these new data sets are providing insights into the continental responses to global climate change (e.g. Williams et al., 1997; Fritz et al., 2004; Scholz et al., 2007, 2011-this issue).

Marine tropical climate records have generally shown the dominance of precession forcing over orbital time scales (Pokras and Mix, 1987; Clemens et al., 1991; deMenocal, 1995). Eolian dust records offshore the coasts of West and East Africa demonstrate the influence of the high latitudes on African climate, but generally show that orbital precession controlled monsoonal climate throughout these intervals (deMenocal, 1995). Pokras and Mix (1987) observed the offshore transport of the freshwater diatom *Melosira* as an indication of African aridity, with spectral analysis of the data showing a strong 23 kyr signal. Clemens et al. (1991) documented strong coherence between Indian Ocean tropical monsoon tracers and the precession cycle. A subtropical continental climate record from the Pretoria Saltpan extends continuously to ~200 ka, where the precession signal dominates the rainfall-derived record (Partridge et al., 1997). Climate modeling demonstrates that meridional and zonal heating gradients in the tropics are greatly affected by precessional forcing (Clement et al., 2004), and are amplified during periods of high eccentricity.

Prior to lake drilling, available tropical continental data sets were either short (e.g. Broecker et al., 1998; Johnson et al., 2002) or of low resolution (e.g. Hooghiemstra et al., 1993; Olsen and Kent, 1996). Prior efforts focusing on climate records from Lake Malawi, generated from sediment cores collected in the 1980s and 1990s (Finney and Johnson, 1991; Johnson et al., 2002; Filippi and Talbot, 2005), record a short but variable climate record over the past 25 ka. These studies, as well as several others, document dry East African climate during the well-known recent high-latitude cold intervals of the Last Glacial Maximum

* Corresponding author.
E-mail address: rplyons@syr.edu (R.P. Lyons).

0031-0182/$ – see front matter © 2009 Elsevier B.V. All rights reserved.
doi:10.1016/j.palaeo.2009.04.014

(LGM), the Younger Dryas, and the Little Ice Age (Gasse et al., 1989; Johnson et al., 1996; Johnson et al., 2002; Brown and Johnson, 2005; Filippi and Talbot, 2005; Powers et al., 2005; Castañeda et al., 2007; Felton et al., 2007; Russell and Johnson, 2007). Some East African climate records extend further back in time, including a core from Lake Tanganyika's Kavala Ridge with an estimated 100 kyr record (Scholz et al., 2003, 2007; Burnett et al., 2011-this issue). In equatorial East Africa, punctuated records from the central Kenya rift extend over the last 175 ka (Trauth et al., 2001; Trauth et al., 2003). Several very long (>1 Ma) discontinuous low-resolution records have been collected throughout Kenya, Ethiopia and Tanzania, as well (Trauth et al., 2005 and references therein). To further investigate East African climate within a context of orbital forcing, high-resolution continuous climate records are needed beyond a single precession cycle (23 ka). In order to understand these orbital forcing mechanisms, the 2005 Lake Malawi Drilling Project collected 623 m of continuous drill core, covering 2 drill sites, and collected a single drill core ~390 m below the lake floor (Scholz et al., 2011-this issue).

Lake Malawi is a useful site for studying long-term (>25 ka) climate change due to its thick sedimentary section (>4 km) (Flannery, 1988; Specht and Rosendahl, 1989) and its great water depth (700 m maximum). This basin configuration probably prevented the lake from experiencing long periods of desiccation throughout the late Quaternary. Furthermore, it allows for the development of anoxic bottom waters beneath ~200 m (Vollmer et al., 2005), which minimize bioturbation, and accordingly preserve annual varves over extended parts of the sediment record (Pilskaln and Johnson, 1991; Johnson et al., 2002).

Seismic-reflection data provide 2-D and 3-D perspectives of lake stratigraphy and allow assessments of depositional variability. Using the principles of seismic sequence stratigraphy, base-level history reconstructions can be developed (Vail et al., 1977; Scholz, 2001). Base-level change in rift basin lakes is controlled by lake-level fluctuations, tectonic subsidence and sediment supply. These changes are manifested in seismic-reflection data as unconformities such as onlap, downlap, and erosional truncation surfaces. However, the use of seismic sequence stratigraphic analysis can only document relative changes in base level, and provides no quantitative age information on sequence stratigraphic development. Whether a given sequence boundary is caused by eustatic (lake level) change, uplift/subsidence, sediment supply variability, and/or compaction (Vail et al., 1977; Reynolds et al., 1991) can be difficult to differentiate. This is especially true in lacustrine rift basins, where subsidence and lake-level fluctuations can occur more rapidly than on marine passive margins (Scholz, 2001).

Previous seismic-reflection studies of Lake Malawi provide evidence for high-magnitude base-level changes that impact the stratigraphic record. Deep basin-scale multichannel reflection profiles were collected during Project PROBE and were used to interpret basin-scale rifting processes and stratigraphy (Rosendahl, 1987; Versfelt and Rosendahl, 1989; Specht and Rosendahl, 1989; Flannery and Rosendahl, 1990; Scholz et al., 1990). Basin-wide stratigraphic unconformities observed in Lake Malawi and neighboring Lake Tanganyika are thought to have been induced by severe low lake stages (Scholz and Rosendahl, 1988; Finney et al., 1996; Scholz et al., 2003). High-resolution imaging of some of the lake's many delta systems, including abandoned delta deposits offshore of the Songwe (Buoniconti, 2000) and Dwangwa Rivers (Martin, 1997) were identified in water depths as much as 500 m below present lake level (BPLL), providing evidence for the lake's high sensitivity to tectonic and climatic change (Scholz, 1995c). Furthermore, evidence for cyclic stacking of sublacustrine fans offshore of the South Rukuru River is thought to have been controlled in part by lake level (Scholz, 1995c; Soreghan et al., 1999). Prior to scientific drilling in 2005, no coring programs had recovered samples deep enough for dating these ancient features observed in seismic profiles.

The objectives of this study are to further constrain the framework developed through interpretation of seismic-reflection data alone, and to gain an understanding of how orbital-scale climate variability in the tropics affects the temporal and spatial variability of seismic- and lithofacies within the Lake Malawi Rift Basin. We present geochemical and geophysical analyses to constrain the timing of sedimentological response to changes in lake level in Lake Malawi over the past ~150 ka, and show how variations in orbital insolation force lake-level change within the basin. Initial reports of the upper ~150 ka of the sedimentary section are found in Scholz et al. (2007), Cohen et al. (2007), and Brown et al. (2007). This paper presents a seismic stratigraphic synthesis of new and existing seismic-reflection data, seismic–drill-core correlations, and a lithostratigraphic summary of each drill site.

2. Geologic setting

2.1. Tectonics and structure

The East African Rift System (EARS) is a north–south alignment of rift basins on the east side of Africa (Fig. 1), that defines the incipient Africa–Somalia plate boundary (Chu and Gordon, 1999). A continuum of extensional processes define the EARS, from rift-related seismicity and minor subsidence in southern Botswana (Wright et al., 2003) to fully developed sea floor spreading in the Afar region to the north (e.g. Yirgu et al., 2006). The EARS is divided into two structural branches (Fig. 1), both oriented in a general N–S direction. The Lake Malawi Rift is located at the southern end of the western branch of the EARS between 9°–14° South. Rifting propagated north to south ~35 Myr ago in the Afar region until it impinged on the edge of the Tanzanian Craton, which is a piece of Archean crust at the center of the East African Plateau (Nyblade and Brazier, 2002). Due to the rigidity of the old, cold craton, the extensional stress of the rift was transmitted to the west 12–10 Myr ago, across the craton into what is now Uganda (Nyblade and Brazier, 2002). Rifting continued to propagate throughout the western branch, including the Malawi rift system.

The total amount of extension is small (~10 km) throughout much of the rift system (Ebinger, 1989). The western branch rift topography is characterized by long-lived half-graben basins associated with steeply-dipping border faults (Specht and Rosendahl, 1989). Along strike of the rift, the border faults alternate in dip polarity across adjacent segments and link across “transfer zones” or “accommodation zones” where strain is transferred (Rosendahl, 1987; Morley et al., 1990). Linkage geometries between the border faults strongly influence the drainage and sedimentation patterns in the basin (Scholz et al., 1993; Scholz 1995a). This style of rifting in conjunction with deep subsidence, results in the development of large, long-lived lake basins, which accumulate packages of sediment more than 4 km-thick in some areas (Rosendahl, 1987; Scholz and Rosendahl, 1988).

Rift orientation is thought to be controlled in part by pre-existing lineaments associated with cratons, mobile belts, earlier rift structures, pre-rift sutures, and basement foliations (Versfelt and Rosendahl, 1989; Ring, 1994; Morley, 1999). The rift utilizes the pre-existing structures to accommodate strain across the rift at transfer zones (Versfelt and Rosendahl, 1989). Boundary faults and accommodation zones in Malawi divide the rift basin into three structural basins (Fig. 1).

2.2. Climate and hydrology

Lake Malawi is one of the largest lakes in the world, at 580 km long, 30–80 km wide and over 700 m deep (Fig. 1). The climate of the Lake Malawi catchment is dominated by annual changes in precipitation–evaporation (P–E) rather than temperature, due to the migration of the Inter-Tropical Convergence Zone (ITCZ). This zone of rising air migrates southward from the equator to the southern reaches of Lake Malawi during the austral summer, bringing moisture from the Indian Ocean, and producing a wet–dry monsoonal cycle, with the wet season extending from December to April. Variations in ITCZ position and

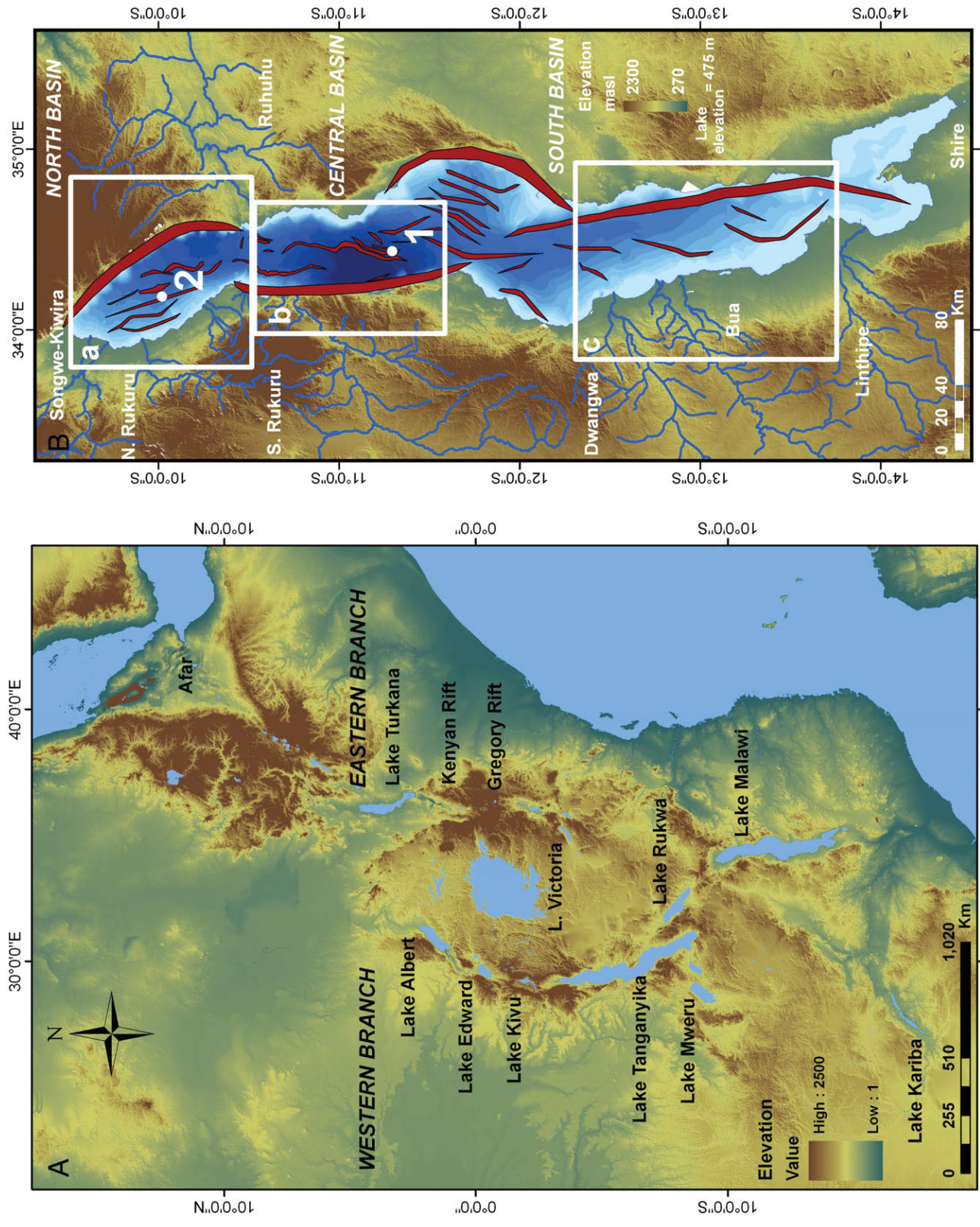

Fig. 1. (A) Digital elevation map based on GTOPO 30 data set (~1 km resolution) of the East Africa Rift System with major rift basins labeled (following Chorowicz, 2005). (B) Hill-shaded 30 m resolution digital elevation model (DEM) based on Satellite Radar Topography Mission (SRTM) data set merged with Lake Malawi bathymetric data from the 392 seismic lines. Drill-site locations are shown and the main fluvial catchments in the Malawi rift valley are also outlined. Major faults (filled in red) separate the three basins, and the white boxes represent panels (A), (B), and (C) in Figs. 2–4.

intensity control the length of the wet season and have contributed to aridity in the Lake Malawi catchment (Johnson et al., 2002; Filippi and Talbot, 2005; Scholz et al., 2007). Regional rainfall is highly seasonal, ranging from >2400 mm/yr in the northern part of the catchment of the lake to <800 mm/yr in higher elevations and regions south of the lake (Malawi Department of Surveys, 1983). This regional variability is influenced by elevation relative to the prevailing wind direction during the wet season, and by proximity to the lake shore.

The lake's water budget is controlled by three major components: precipitation, evaporation, and outflow (Kidd, 1983; Kingdon et al., 1999). Precipitation is either in the form of direct rainfall onto the lake, or rainfall in the catchment which flows into the lake as runoff. Evaporation from the lake's surface is the main component of the lake's water loss (Kidd, 1983; Kingdon et al., 1999). Several drainage systems enter the lake across several different structural settings (Fig. 1), and structural setting is the primary control on inlet catchment size and delta morphology (Scholz, 1995c).

The North Basin is a single half-graben basin with the border-fault margin on the northeastern side associated with the Livingstone Mountains, and the shoaling flexural margin to the southwest (Figs. 1 and 2) (Scholz et al., 1989). The basin has three major fluvial inputs; the Songwe River, the N. Rukuru River, and the Ruhuhu River, with several minor inputs on both sides of the lake (Figs. 1 and 2). The Songwe–Kiwira River system flows along the axis of the rift valley and enters the lake at the north end of the North Basin (Fig. 2). It drains volcanic rocks from the Rungwe volcanic system as well as Karroo and Cretaceous sedimentary rocks (Malawi Department of Surveys, 1983). Precipitation in this catchment is the highest among all of the major Lake Malawi catchments (Malawi Department of Surveys, 1983), and annual inflow into the lake from this system accounts for ~13–14% of the total inflow (Kingdon et al., 1999). The Ruhuhu River system enters Lake Malawi on the eastern shore at the southern edge of the Livingstone Mountains border fault system (Figs. 1 and 2). This river system enters the lake at an accommodation zone (e.g. Rosendahl, 1987) and its drainage area (14,070 km^2) is the largest in the catchment and discharge is the highest of all the rivers in the basin, accounting for ~20% of the total inflow into the lake (Kidd, 1983; Kingdon et al., 1999).

The Central Basin extends for about 150 km in a north–south direction, and is bound on the west side by a two border fault–relay ramp system that dips to the east (Figs. 1 and 2) (Soreghan et al., 1999). The north–northwest dipping Lipichili Fault Zone (LFZ) striking SW–NE cuts through the southern edge of the basin, displacing the water bottom by ~75 m (Fig. 2) (Scholz et al., 1989). The South Rukuru River enters the western edge of the northern part of the basin over the border-fault system, and is thought to be an antecedent drainage system (Fig. 2) (Crossley and Crow, 1980). This river system drains Karroo sedimentary rocks and Precambrian crystalline rocks (Malawi Department of Surveys, 1983), accounting for 4.2% of the total inflow into the lake (Kidd, 1983). Seven kilometers farther north along the western shore, the North Rumphi River flows into Lake Malawi, contributing sediments to the Central Basin in conjunction with the South Rukuru River (Fig. 2).

The South Basin is the largest and shallowest part of Lake Malawi, with maximum water depths of ~400 m adjacent to the border-fault margin on the eastern edge of the lake (Figs. 1 and 2). On the western shoaling, or flexural margin, there are several fluvial inputs, the largest of which include the Dwangwa, Bua, and Linthipi Rivers (Figs. 1 and 2). The Dwangwa River system is the largest in this part of the lake, draining an area of 7650 km^2. The Shire River is the lake's outflow and drains to the south to the Zambezi River; its discharge and depth are highly variable depending on seasonal precipitation. However, the river is relatively shallow (<10 m) and low in discharge (5–10 km^3/yr) (Kingdon et al., 1999).

These hydrologic boundary conditions result in significant annual lake-level changes (~1–3 m) with small variations in rainfall, causing shifts from open- to closed-basin conditions over historical and geological time periods (Spigel and Coulter, 1996). Slight drops in P–E ratio will cause large changes in the lake level of the basin. These amplified changes of catchment and lake-surface conditions are well-recorded in the sediments of the lake (Owen et al., 1990).

3. Methods

3.1. Seismic-reflection surveys

To develop a sequence stratigraphic framework for the entire Lake Malawi Rift Basin, we used over 10,000 km of seismic-reflection profiles collected over the past ~20 yrs (Fig. 3). These data vary in scale from a low-resolution, basin-scale (6-second record length) multichannel data set collected in the 1980s by Project PROBE (Rosendahl, 1987; Scholz and Rosendahl, 1988; Flannery and Rosendahl, 1990), to high-resolution single-channel (2–3 s record length) data sets collected in the mid-90s and in 2001 (Table 1) (Scholz, 1995b; Martin, 1997; Soreghan et al., 1999; Buoniconti, 2000). All data sets were processed using standard techniques with Landmark Graphic's ProMAX processing software (Table 1). Seismic velocities of the water column and the upper sedimentary section of each seismic profile were calculated to be ~1450 m/s by determining first

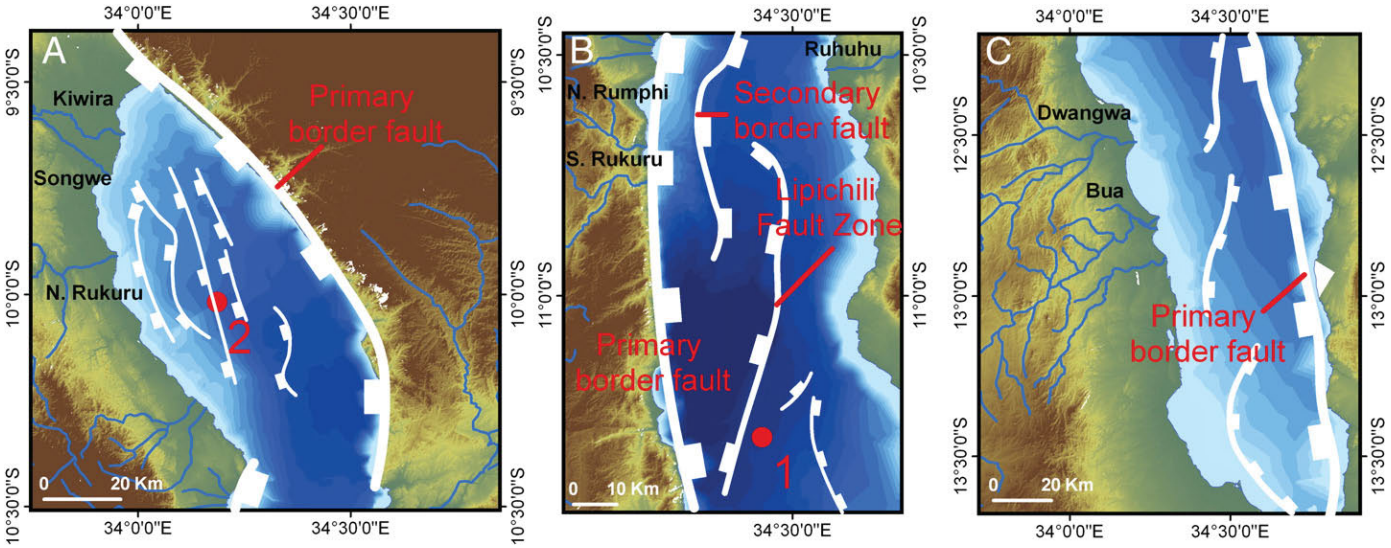

Fig. 2. Maps of each of the basins in Lake Malawi (A–C), showing major border faults and intrabasinal fault zones.

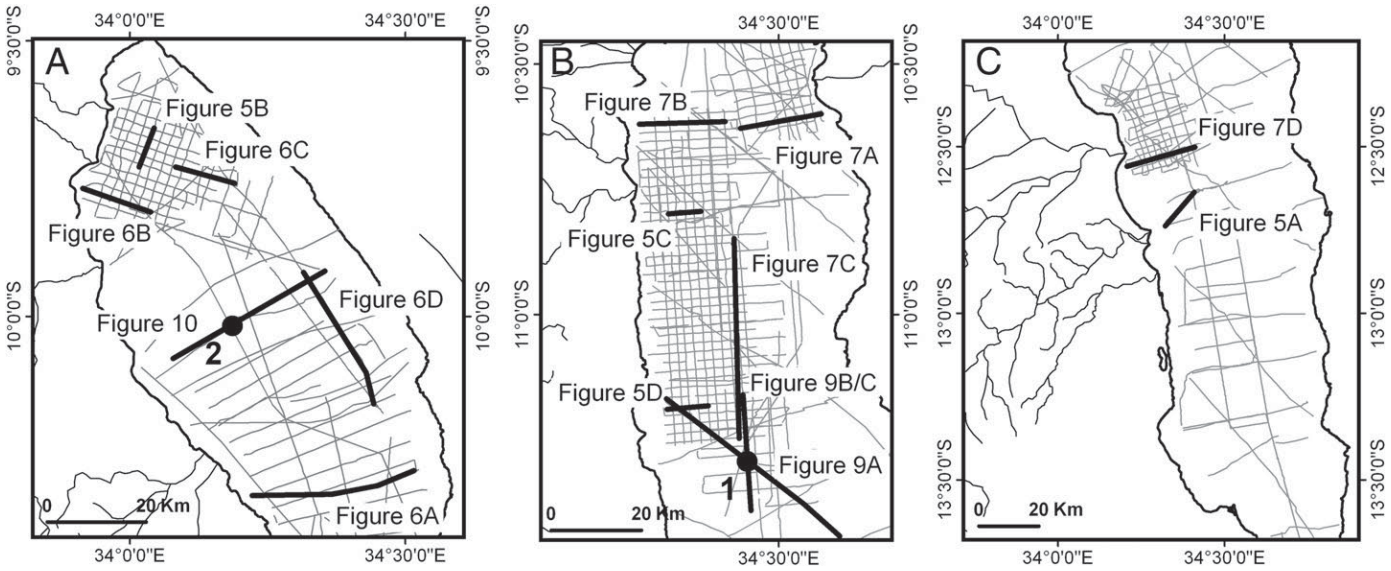

Fig. 3. Seismic survey basemap for the North (A), Central (B) and South Basins (C) of Lake Malawi. Seismic-reflection profiles used in this study are labeled. Four vintages of seismic data are represented by these tracklines. Their survey parameters are listed in Table 1.

return water-bottom velocities using multichannel seismic data. This value was confirmed by comparing the time–depth relationship of the water bottom on the seismic-reflection profiles and the associated driller logs at each 2005 drill site.

Seismic stratigraphic analysis was performed using Landmark Graphic's SeisWorks 2-D interpretation software. We applied the principles of sequence stratigraphy by identifying stratal terminations and defining depositional sequences in seismic-reflection profiles (Vail et al., 1977). Within sequences, the exact positions of paleo-shorelines can be defined by ancient delta deposits associated with major rivers that enter the lake. Sequence boundaries defined by toplap, downlap, onlap and erosional truncation were interpreted and correlated to the drill sites.

3.2. Seismic facies framework

A variety of acoustic facies are observed on seismic-reflection profiles in the basin (Figs. 4 and 5). Seismic facies in large, deep rift valleys have been described previously (e.g. Lezzar et al., 1996; Martin, 1997; Back et al., 1999; Soreghan et al., 1999; Buoniconti, 2000; Colman et al., 2003; McGlue et al., 2006). In order to integrate interpretations from the various seismic data sets, we use a simplification of the facies types described by those authors.

Hemipelagic drape facies consists of continuous reflections of either high or low-amplitude that are generally flat-lying and can be observed blanketing or onlapping pre-existing features on the lake floor (Fig. 5A). This facies consists of detrital silt and clay with variable

Table 1
Lake Malawi seismic-reflection survey parameters.

Year	MCS/SCS	Total acquisition distance (km)	Line spacing (km)	Source	Bandwidth (Hz)	Receiver	Acquisition system	Record length (s)	Sample rate (ms)	Processing parameters	Positioning	Published papers
1986–1987	24 fold MCS	>3500	~25–50	40–140 in^3 single airguns or multigun arrays	8–128	960 m long, 48 channel GECO cable, 1 m phone spacing, 20 m group interval, 440 m lead-in	Texas Instruments DFS V	6	2	Demulitplexing, F-K filtering, deconvolution, velocity analysis, normal moveout, CDP stacking, band-pass filter (8/10–40/55 Hz)	TRANSAT satellites and radar; GPS used ~20% of acquisition time	Scholz and Rosendahl, 1988; Flannery, 1988; Flannery and Rosendahl, 1990
1992	SCS	2100	2	5–10 in^3 airgun or 15 in^3 watergun	50–500	50-element Teledyne hydrophone streamer	MASSCOMP computer	2	0.5	SIOSEIS software — band-pass filter (50–500 Hz), edits, mutes, 100 ms AGC	Autonomous GPS — 15 m resolution — acquired every~6 s	Scholz et al., 1993; Scholz, 1995
1995	SCS	>2000	2	12 in^3 Bolt 600B airgun — 2000 psi	80–700	ITI 10-phone solid towed array	Elics-Delph 2	2	0.5	Promax software — 3-trace horizontal stack, band-pass filter (80–500 Hz), 100 ms AGC, trace balancing	Autonomous GPS — acquired every ~5 s	Soreghan et al., 1999
2001	SCS	1840	2	10 in^3 and 20 in^3 Bolt 600B airgun — 2000 psi	50–450	S.I.G. 10 m 16 hydrophone element streamer	Elics-Delph 2	3	0.5	Promax software — 3–trace horizontal stack, band-pass filter (80–500 Hz), 100 ms AGC, trace balancing	Continous Autonomous GPS	Unpublished

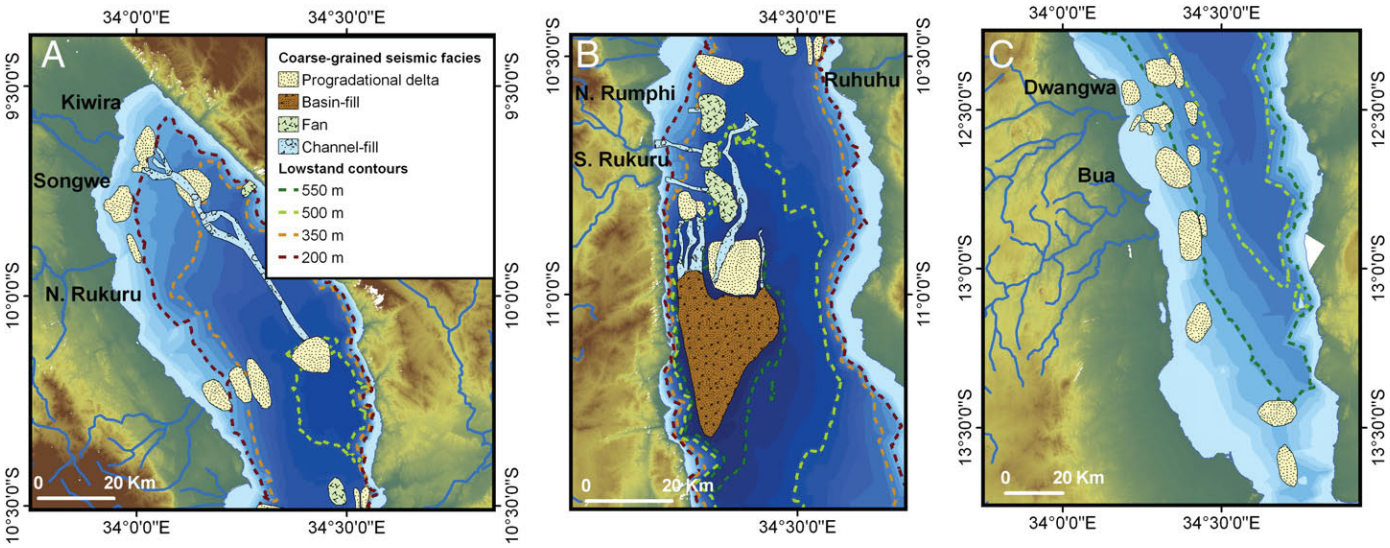

Fig. 4. Distribution of coarse-grained seismic facies deposited during the most recent lowstand and subsequent transgression (Sequence I), mapped throughout each of the three structural basins of the lake (A–C). Key bathymetric contours associated with main low lake stages are highlighted (−550 m, −500 m, −350 m, and −200 m below modern lake level) and major fluvial inputs are labeled.

amounts of biogenic silica, diatoms, ostracodes, organic matter, and carbonate sediment (e.g. Johnson and Ng'ang'a, 1990; Pilskaln and Johnson, 1991; Johnson et al., 2002).

The internal geometry of *progradational delta facies* typically contains sigmoid or oblique clinoform reflections (Fig. 5A), where reflections downlap onto lower bounding surfaces and toplap onto upper bounding surfaces. Externally, the facies appear lobate on dip-oriented seismic profiles. Hemipelagic drape facies commonly onlap the down-dip edge of the clinoform sets (Fig. 5A). Progradational delta facies in Lake Malawi can reach thicknesses of ~50 m and can cover areas of ~100 km^2 (Martin, 1997; Buoniconti, 2000). Piston and vibro-cores of these features in both the North and South Basins have

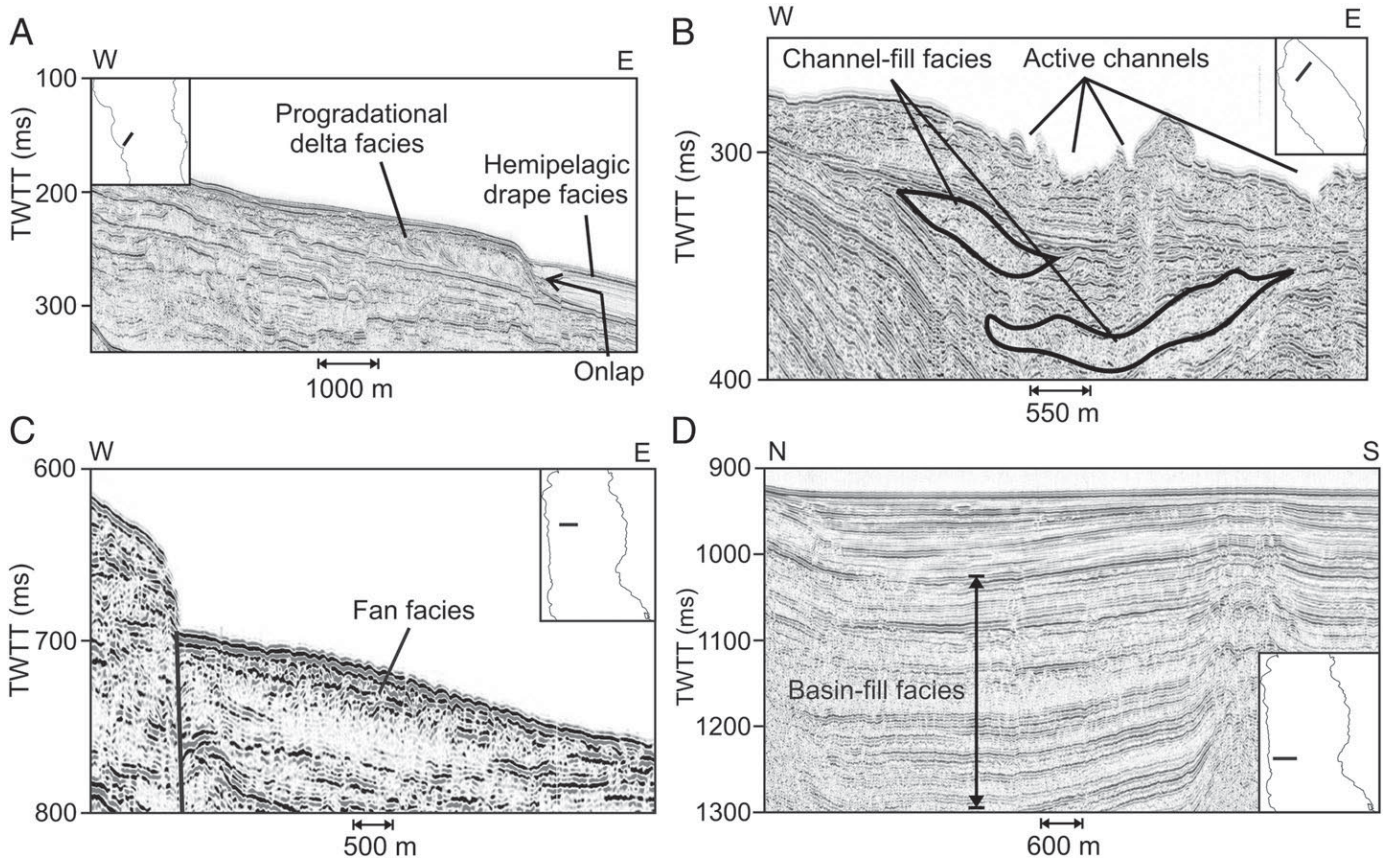

Fig. 5. Seismic-reflection profiles showing seismic facies. (A) Progradational delta facies from the South Basin, near the Dwangwa Delta (following Scholz, 1995b; Martin, 1997). Seismically-transparent hemipelagic drape facies onlap the delta from the east. (B) Active channels and channel-fill facies from the North Basin of the lake (following Buoniconti, 2000). (C) Fan facies from the mouth of a sublacustrine canyon offshore the S. Rukuru River in the Central Basin (after Scholz, 1995b; Soreghan et al., 1999). (D) Basin-fill facies from the depocenters of the Central Basin in ~700 m of water.

revealed coarse-grained sands and gravels (Butch, 1996). The clinoforms found in Lake Malawi are similar to depositional shelf clinoforms in morphology (e.g. Cathro et al., 2003; Fulthorpe and Austin, 2008; Monteverde et al., 2008; Xie et al., 2008) but differ in both spatial and vertical scales.

Channel-fill facies comprise discontinuous to chaotic low-amplitude reflections that may terminate against each other (Fig. 5B). High-amplitude reflections mark the bounding surfaces of these features. Externally, channel-fill facies are often "U-shaped" in cross-section but upper bounding surfaces can be hummocky. Sediment cores of channel-fill facies contain fining-upwards packages and coarse-grained gravity-flow deposits (Wells et al., 1999). Soreghan et al. (1999) also observed such facies in the Central Basin of Lake Malawi.

Fan facies are wedge-shaped deposits with planar basal surfaces in down-dip view and are internally chaotic (Fig. 5C) (Soreghan et al., 1999). Sediment core samples from these deposits indicate they consist of coarse-grained mass-flow deposits with minimal internal grading (Wells et al., 1999). This facies includes mouth-of-canyon fan facies and fan delta facies observed by Soreghan et al. (1999).

Basin-fill facies generally occur in the depocenters of each basin and are characterized by discontinuous internal reflections with high-amplitude variability (Fig. 5D). Externally they consist of basal onlapping reflections and coring of these facies reveals hemipelagic mud and turbidites (Soreghan et al., 1999; Wells et al., 1999; Buoniconti, 2000).

3.3. Paleo-water depth estimations

We use observations of prograding clinoform reflections to determine past shoreline positions and to reconstruct the lake-level history. Past lake levels are assessed by measuring the depth of topset–foreset break point below modern lake level. This approach requires two assumptions: (1) The clinoform break point defines, or is in proximity to, a paleo-shoreline. This approach has been used extensively in other settings, and has been validated in numerous case studies in both marine and lacustrine environments. Aksu et al. (1992) used the topset–foreset transition of prograding clinoforms observed in seismic-reflection data in the eastern Aegean Sea to define ancient paleo-shorelines. Driscoll and Karner (1999) modeled 3-dimensional development of river-mouth clinoforms based on sediment supply and subsidence where the clinoform break point is located proximal to the shore line. Metzger et al. (2000) referred to the clinoform break point as the clinoform rollover, and modeled the rollover as close to base level. Saller et al. (2004) observed cyclic deltaic sedimentation as a function of changing sea level offshore India. McGlue et al. (2006) also used the topset–foreset transition of a lowstand delta in Lake Edward, East Africa to define a paleo-shoreline when drainage patterns of the region were different than today. (2) Sedimentation rate and subsidence rate are equal during subsequent sedimentation and burial following lowstand delta deposition. Maximum subsidence rates have been calculated at 0.5–1 mm/yr in the western branch of the EARS (Einsele, 2000). Average sedimentation rates in the Lake Malawi basin are ~1 mm/yr (Pilskaln and Johnson, 1991; Johnson et al., 2002). Whereas the reliability of these estimates is diminished for the deeper, older parts of the stratigraphic section, there is no evidence for major changes in those processes since the mid-Pleistocene.

3.4. Drill-core data

Details of the drilling program and core collection are described in Scholz et al. (2006) and Scholz et al. (2011-this issue). Whole-core geophysical properties measurements of GRAPE density (Gamma-Ray Attenuation Porosity Evaluator), sonic velocity (1 cm sample intervals) and natural gamma (NGR) (16 cm sample intervals) were made using a Geotek multi-sensor logger at the Limnological Research Center (LRC) at the University of Minnesota. Preparation and analyses of total organic carbon (TOC) are described in Scholz et al. (2007) and Scholz et al. (2011-this issue). Because of occasional gaps in the unconsolidated sediment within some core sections, values of saturated bulk density measured via the GRAPE method were <1 g/cc within some core sections. A filter was applied to the data set to remove any values <1 g/cc, and then a 15-point running average was applied to the data. The 15-point running average also removes any small-scale variability not representative of core lithology. Natural gamma plots were filtered to remove values <15 counts/s (cps). The sonic velocity logs show highly variable values, but with several values below 1400 m/s. These are probably due to poor coupling between the drill-core liner and sediment when measured in the GEOTEK logger. We applied a 1400 m/s filter to remove low values from the data set, reducing the range of the data set to between 1400 and 1700 m/s. Stratigraphic columns of each drill site were constructed from original core descriptions and subsequent inspection of high-resolution digital imagery of the cores acquired using a Geotek Geoscan-V and a DMT CoreScan Colour scanner. To develop seismic–drill-core correlations beneath the lake floor, we utilized the sonic velocity logs and correlated large amplitude shifts in the seismic-reflection data to large variations in the lithology of the cores using the digital imagery, stratigraphic columns, geophysical and geochemical properties as guides. Details of the age model applied in this study are presented in Scholz et al. (2007), Brown et al. (2007), and Scholz et al. (2011-this issue).

To determine the control on seismic amplitude in the near subsurface, we developed synthetic seismograms from the upper ~75 m of Drill Site 1B using Jason™ wavelet generation software, where whole-core sonic velocity and density data from the drill site were used to calculate reflection coefficients and to estimate a wavelet to convolve those coefficients into synthetic traces. We used sonic velocity and density data from the drill core to invert the seismic data into a profile of acoustic-impedance data, generating a two-dimensional "real-earth" representation of the subsurface, rather than a standard wavelet-filtered perspective. Jason™ software was also used to compute a down-core correlation coefficient between the seismic and synthetic traces, as well as amplitude spectra of the estimated wavelet, seismic-trace data, and drill-site reflectivity series.

4. Results

4.1. Seismic sequence stratigraphy

Each of the three main structural basins in Lake Malawi exhibits unique stratal architecture and seismic facies characteristics due to contrasting structural geometry. There is evidence for considerable amounts of erosional truncation and stratigraphic thinning of sequences in each basin due to both rapid lake-level change and localized rift-related subsidence. Whereas shallow reflections and sequence boundaries can be identified across the basins, the deeper stratigraphy in the North and Central basins is interpreted independently, and stratigraphic correlations are made between them based on consistent similarities in acoustic character and stratal relationships.

4.1.1. North Basin

In the North Basin, we identify progradational delta facies offshore of the Songwe–Kiwira River system in single-channel seismic-reflection data (Figs. 4 and 6). These clinoform packages are evidence for low lake stages (Figs. 4 and 6) (Buoniconti, 2000). A complex system of channels feeds three lowstand delta packages in the eastern part of the basin (Fig. 4). Based upon the previous interpretations of the Project PROBE multichannel seismic data set, the sedimentary fill of the North Basin is divided into three stratigraphic sequences that diverge toward the basin-bounding fault to the northeast (Figs. 2 and 6) (Scholz et al., 1989; Flannery and Rosendahl, 1990). In the higher-resolution seismic data set acquired in this study, we are able to resolve the original upper two sequences into several lake-level cycles. Three sequences are identified here (Sequences 1–III, Fig. 6),

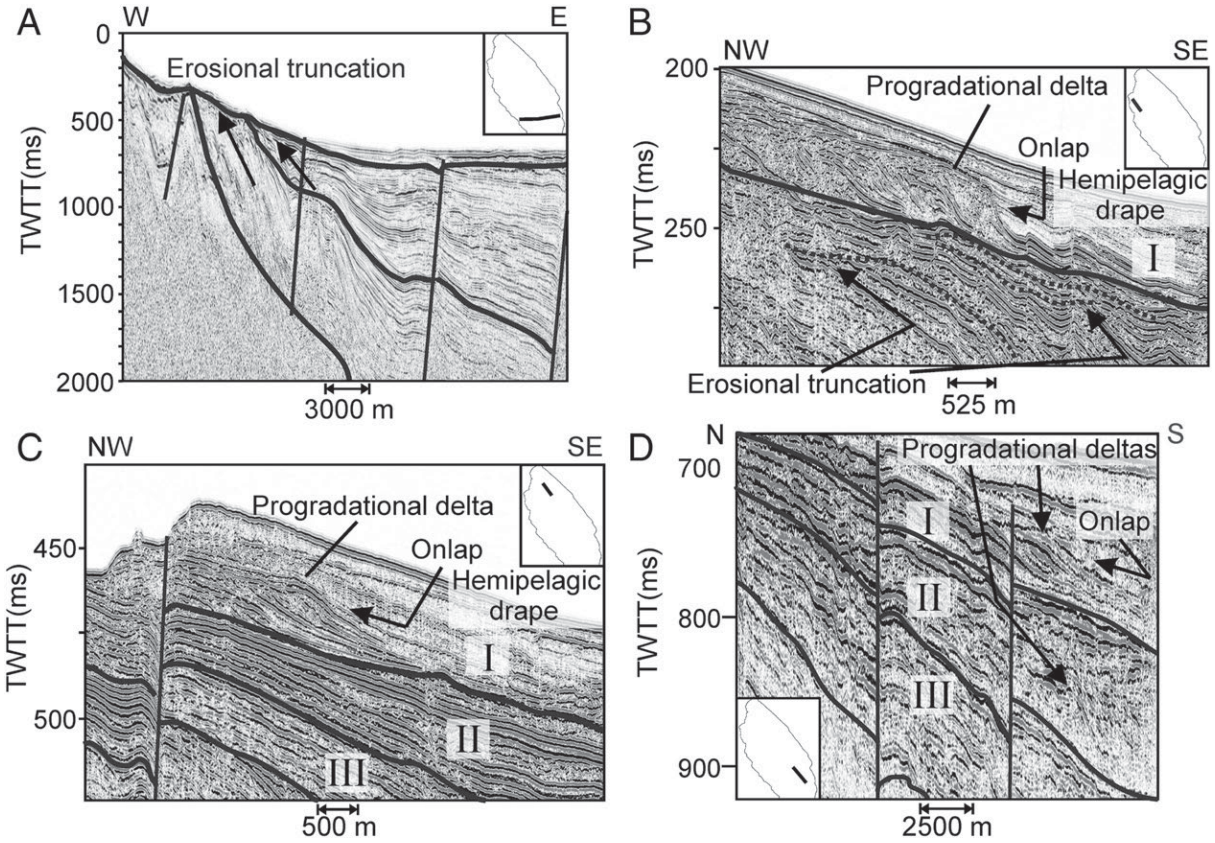

Fig. 6. Seismic-reflection profiles showing evidence of low lake stages in the North Basin. (A) A Project PROBE seismic-reflection profile from the North Basin with the interpreted sequence boundaries developed from the original 1980s multichannel seismic data set (Scholz et al., 1989; Flannery and Rosendahl, 1990). Note the pronounced erosional truncation of sequences on the western shoaling margin of the basin. (B) Seismic-reflection profile of the progradational reflection package during Sequence I, interpreted as a lowstand delta, which in part defines the position of the shoreline and the lower lake stage at −200 m below modern lake level. Sequences II and III are not present in this locality, but evidence for extensive erosional truncation of previous intervals is observed. (C) Progradational seismic-reflection package, interpreted to be a lowstand delta that defines the −350 m lowstand during Sequence I. (D) Seismic-reflection profile showing two low-aspect ratio progradational packages, interpreted to reflect the shoreline position and the two −500 m lowstand events within Sequences I and II.

each representing a complete lake-level cycle that exhibits both lowstand and highstand seismic facies. The sequences are bounded by erosional truncation surfaces and high-amplitude continuous reflections that are interpreted as erosional surfaces.

Sequence I is the youngest sequence observed in the data set and marks the most recent lake-level cycle, beginning with a 500 m lowstand marked by a lowstand delta deposit (Figs. 4 and 6). Internally, this oblique clinoform is characterized by prograding foreset beds truncated at their tops. Delta-foreset slopes are ~0.8°. Externally this package is lobe-shaped, and characterized by a ~30 m-thick package bounded by high-amplitude reflections. Seismically-transparent continuous reflections typical of the hemipelagic drape facies onlap the southern edge of the clinoform package (Fig. 6D). Following the low lake stage, water levels rose, and two prograding clinoform packages were deposited at 350 and 200 m BPLL (Fig. 6B and C). The −350 m delta's internal geometry is sigmoid–oblique, and externally, this ~30 m-thick clinoform package is displaced by a normal fault (Fig. 6). It covers 50 km^2 and its foresets dip at ~2.5°. Hemipelagic drape facies onlap the edge of the delta package (Fig. 6C). The −200 m delta package is ~32 m-thick, the foresets dip at ~8.0°, and it covers 53 km^2 (Figs. 4 and 6). The source of these three delta deposits was the Kiwira River, the main channel of which is now part of a sublacustrine channel complex (Fig. 4). Toplap and downlap surfaces of the −200 m delta are correlated to additional ~46 m-thick clinoform package offshore of the Songwe River in 200 m of water (Fig. 6B). This progradational package is characterized internally by sigmoidal clinoforms with high-amplitude internal reflections. It covers ~57 km^2 and its foresets dip at ~5.5° (Figs. 4 and 6). Similar to the other deltas deposited during this transgression, hemipelagic drape facies onlap the leading edge of the clinoform package (Fig. 6A). Evidence for this transgression is also observed on the western shoaling margin (Fig. 4). Here, deltas back-step from 500 m, to 350 m and finally 200 m BPLL. The base of this sequence marks a basin-wide unconformity correlative to the base of the upper sequence on the PROBE seismic-reflection profiles (Fig. 6A) (Scholz and Rosendahl, 1988; Scholz et al., 1989; Flannery and Rosendahl, 1990; Finney et al., 1996; Scholz et al., 2003).

Sequence II represents the previous lake-level cycle, also beginning with a −500 m lowstand delta package (Fig. 6D). This oblique clinoform package has an eroded toplap surface but is generally chaotic internally. This seismic character may be due in part to penetration limitations of the high-resolution seismic acquisition system. The magnitude of the highstand component during Sequence II is unknown; however, a delta deposit is observed at 300 m BPLL (Fig. 4). Much of this sequence is eroded above the 300 m level, probably due to the subsequent lowstand at the beginning of Sequence I. This prograding clinoform package within Sequence II indicates that highstand magnitude reached at least 300 m BPLL.

Sequence III is the oldest, deepest sequence studied, and is only identified by bounding high-amplitude surfaces in the deeper parts of the basin (Fig. 6C and D). No ancient deltas are observed within this sequence; accordingly, identification of the lake-level extent of this sequence is remains equivocal. However, this sequence is similar in thickness to Sequence II and is bounded by high-amplitude continuous reflections.

Offshore of the Ruhuhu River system, the base of Sequence I is an erosional surface overlain by onlapping transparent continuous reflections (Fig. 7A). The most recent transgression is manifested here by the onlapping reflections. Also within this sequence, seismically transparent packages bounded by high-amplitude continuous reflections spill into the southern edge of the North Basin (Fig. 4). These are interpreted as lowstand fan deltas deposited at the beginning of Sequences I and II. Also during Sequence II, fan delta packages that dip into the Central Basin are observed in ~450 m of water (Fig. 7A). Even with the high sediment supply from the Ruhuhu River, aggradation rather than progradation dominates these fan deltas. This is due to the steep slopes associated with the accommodation zone setting (Scholz et al., 1993). Similar packages are observed deeper in the section as well (Fig. 7A). Due to the structurally controlled broad anticline or transverse fold (following Schlische, 1995) offshore of this river system, basin-switching of fan deltas between the North and Central basins is probably a common process of coarse-grained sedimentation at this locality.

4.1.2. Central Basin

In the Central Basin, sedimentation is directed south towards the hanging wall of the Lipichili Fault Zone (LFZ), the deepest part of the lake, down the relay ramp from the South Rukuru River, or by a long sublacustrine channel from the Ruhuhu River (Figs. 2 and 4). The sedimentary section expands on the hanging wall of the LFZ. Much of the section here consists of basin-fill facies deposited from the north (Fig. 7C). The footwall side of the LFZ consists of mostly profundal hemipelagic drape facies, due to limited detrital inputs into the area.

The South Rukuru and North Rumphi River systems feed sublacustrine channels that transport coarse-grained material to the edge of the secondary border fault (Figs. 2 and 4). There, canyons incise the border fault and feed vertically- and laterally-stacked sublacustrine fans (Fig. 7B). Soreghan et al. (1999) proposed that the occurrence and spatial distribution of these fans is indicative of lake-level fluctuations, with highstands associated with high-amplitude continuous reflections interpreted as hemipelagic drape facies and lowstands associated with low-amplitude fan facies. The three sequences from the North Basin are also interpreted here, marking three successive units of a basal fan facies deposited above seismically transparent hemipelagic drape facies. Several more lake-level cycles can be identified in seismic profiles here than are observed in the North Basin (Fig. 7B).

4.1.3. South Basin

In the South Basin, large clinoforms interpreted to be lowstand delta deposits are present offshore and show the same transgression as the North Basin, although with no record of the most severe (−500 m) lowstands, as maximum water depth is only ~400 m. Progradational delta facies are prevalent throughout this basin (Fig. 4). Offshore of the Dwangwa River, a series of these deposits is identified within Sequence I, characterizing the last transgression, and is manifested here as a series of back-stepping prograding clinoform

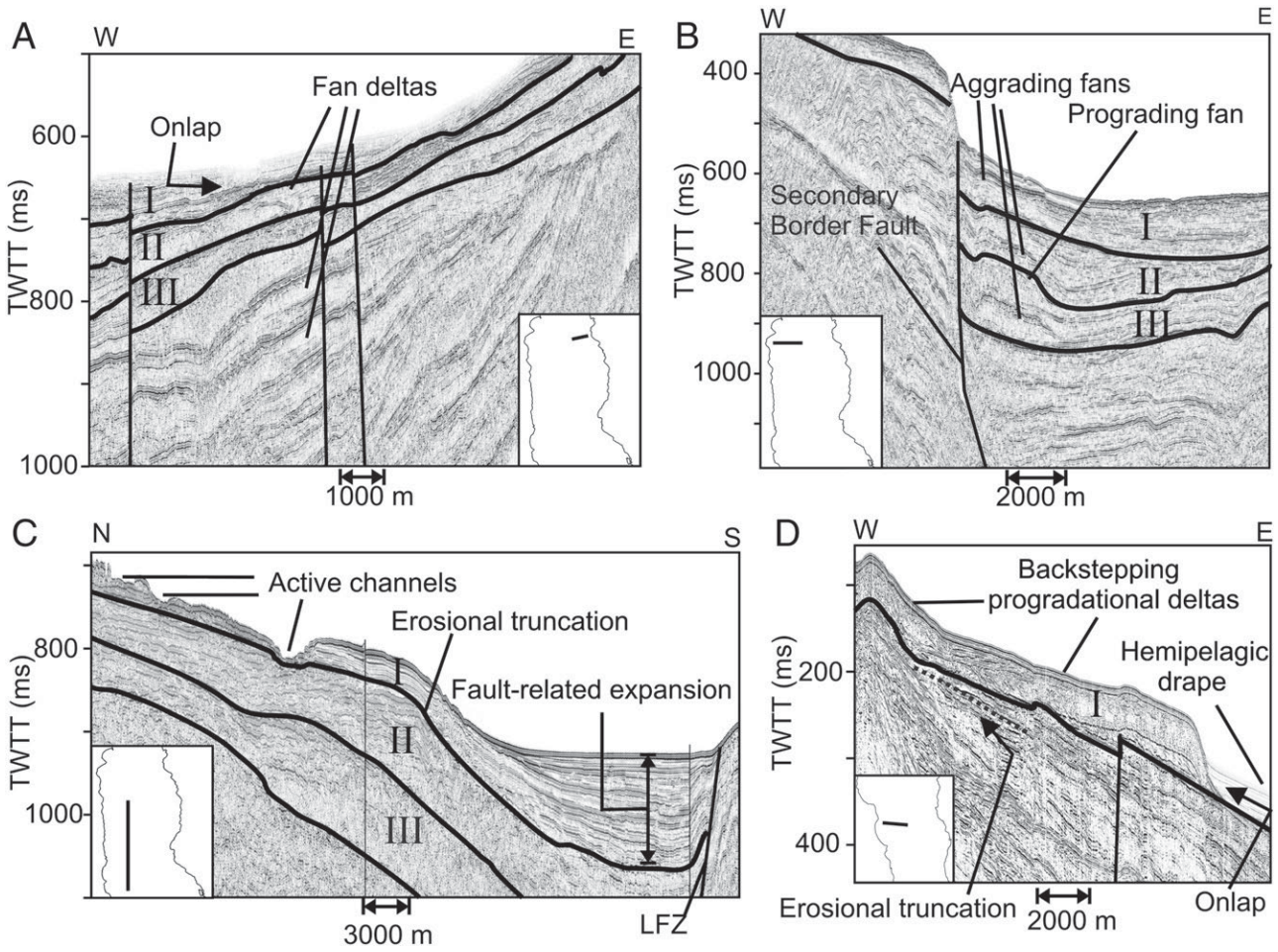

Fig. 7. (A) Lowstand fan deltas in 500 m modern water depth offshore of the Ruhuhu River system, an accommodation zone fluvial system. (B) Seismic line showing stacked mouth-of-canyon fans in the Central Basin of Lake Malawi (C) A seismic-reflection profile from the Central Basin demonstrating the expansion of sequences towards the LFZ. The presence of modern active channels on the northern part of the profile suggests episodes of channelization during periods of lower lake level. (D) Lowstand delta in 200 m of water associated with the Dwangwa River system in the South Basin.

packages observed from 300 m to 200 m to 100 m and finally 75 m BPLL (Fig. 7D). The −200 m clinoform package is the largest ancient preserved delta in the entire lake, covering more than 100 km^2 (Martin, 1997). This package contains well-developed, oblique clinoform reflections and a lobate external geometry typical of the deltas seen in seismic profiles throughout the rest of the lake (Figs. 4 and 6) (Martin, 1997). There is also evidence for several ancient deltas in as much as 200 m of water farther south along the flexural margin, offshore of other rivers on the western margin of the basin (Fig. 4). Two −200 m clinoform packages prograde north from the southern edge of the basin (Fig. 4), providing evidence for a southern axial input when the basin was closed. This system may have been fed by the Linthipe River which now enters at the southwestern edge of the lake (Fig. 1).

4.1.4. Delta-foreset variability

We plot clinoform foreset angles of 10 lowstand delta deposits identified in Lake Malawi seismic-reflection profiles versus their lowstand magnitude (Fig. 8). To determine the true dips of each clinoform foreset, we subtracted background depositional slopes from the apparent dips of each clinoform foreset on seismic-reflection profiles oriented perpendicular to the progradation direction. We observe a trend of increasing foreset dip with decreasing lowstand magnitude (Fig. 8).

4.2. Seismic drill-core correlation

Drill Site 1 is situated on the footwall block of the LFZ in 592 m of water (Figs. 1 and 9). This location in deep water was chosen because of its thick, undisturbed, and continuous sedimentary section, its isolation from deep water turbidites, and because it was probably never subaerially exposed during lake lowstands (Figs. 2 and 4) (Scholz et al., 2011-this issue). Drill Site 2 is located in the North Basin in 359 m of water (Fig. 1). A seismic-reflection profile here reveals a ~35 m-thick section of transparent hemipelagic drape facies, with a high-amplitude reflection at its base (Fig. 10).

4.2.1. North Basin Drill Site 2

The seismic profile over this site indicates a ~35 m-thick package of seismically transparent hemipelagic drape facies over a series of continuous high-amplitude reflections (Fig. 10). On the seismic-reflection profile, the uppermost ~15 ms contain continuous high-amplitude reflections, and digital images of the drill cores show that this section contains laminated brown mud (Fig. 10). Seismic reflectivity of the hemipelagic drape facies is reduced further down in the section (~475–~505 ms two-way travel time (TWTT)), and is associated with cores lacking laminations (Fig. 10). At the base of the section, a high-amplitude reflector correlates to a sharp change in density.

The hemipelagic drape facies are subdivided into three lithofacies based on correlations to the cores (Fig. 11). The upper section consists of moderately organic-rich (2–4%), low density (~1.2 g/cm^3) diatomaceous mud with sparse laminations. Farther down in the section (~505 ms–~515 ms TWTT), finely-laminated mud is observed, where TOC values increase markedly to 4–6% or more (Fig. 11). At the base of the hemipelagic drape facies (~520 ms TWTT), GRAPE density increases to 1.7–2.0 g/cm^3, TOC decreases to 0.1–2%, and carbonate- and ostracode-rich mud is present (Scholz et al., 2007; Brown et al., 2007). This interval is also characterized by high values of NGR (Fig. 11). The high-amplitude seismic reflections at the base of the drill site are associated with dense (up to 2.0 g/cm^3), fine- to medium-grained sand in the drill core (Figs. 10 and 11). These sands are located within a series of three coarsening upwards sequences. The presence of the unconformity and the coarsening upwards sequences are evidence that this horizon is an exposure surface, and the sands are indicative of a transgressive shoreface, which developed during the last rise in lake level. The hemipelagic drape facies above this surface is interpreted to be deposited during the subsequent transgression and under higher lake-level conditions. The rapid transition from sediment densities as high as 2.0 g/cm^3 to densities as low as 1.2 g/cm^3 in the drill core is responsible for the dramatic change in seismic amplitude at this boundary.

Sequence II underlies the unconformity but the recovered cores did not penetrate this sequence. Hemipelagic drape facies is observed at the top of this sequence, associated with fine-grained mud (Fig. 10). The base of the sequence is marked by a continuous high-amplitude reflection, similar to the base of Sequence I. We interpret this surface to be the previous transgressive shoreface, which most likely consists of fine- to medium-grained sands.

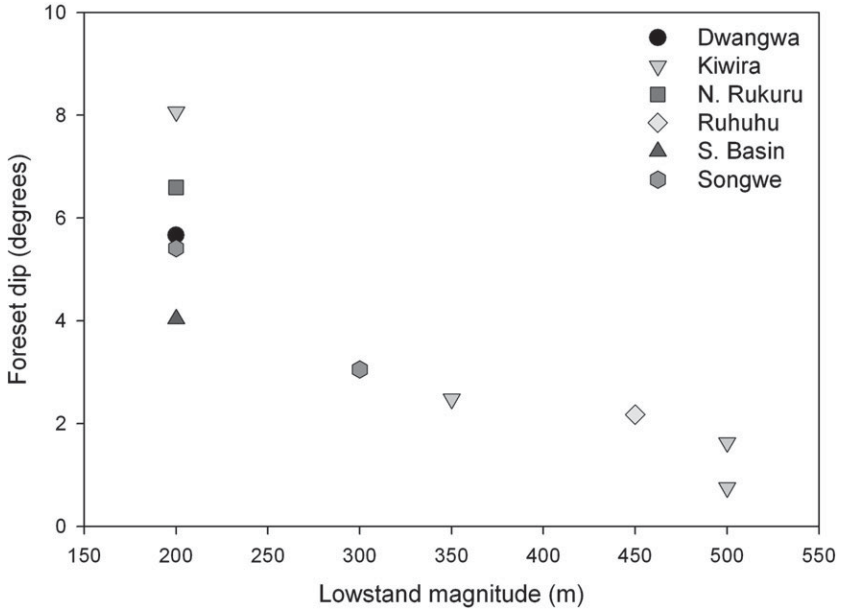

Fig. 8. Foreset dip versus lowstand magnitude of 10 lowstand delta deposits in Lake Malawi. The background depositional slopes of the deltas were measured on the dips of the topsets and bottomsets of each delta from seismic-reflection profiles oriented parallel to dip direction. This slope was subtracted from the measured dip of the foresets to give the true dip of the foresets relative to a flat plane. Foreset dips decrease during the more extreme low lake stages.

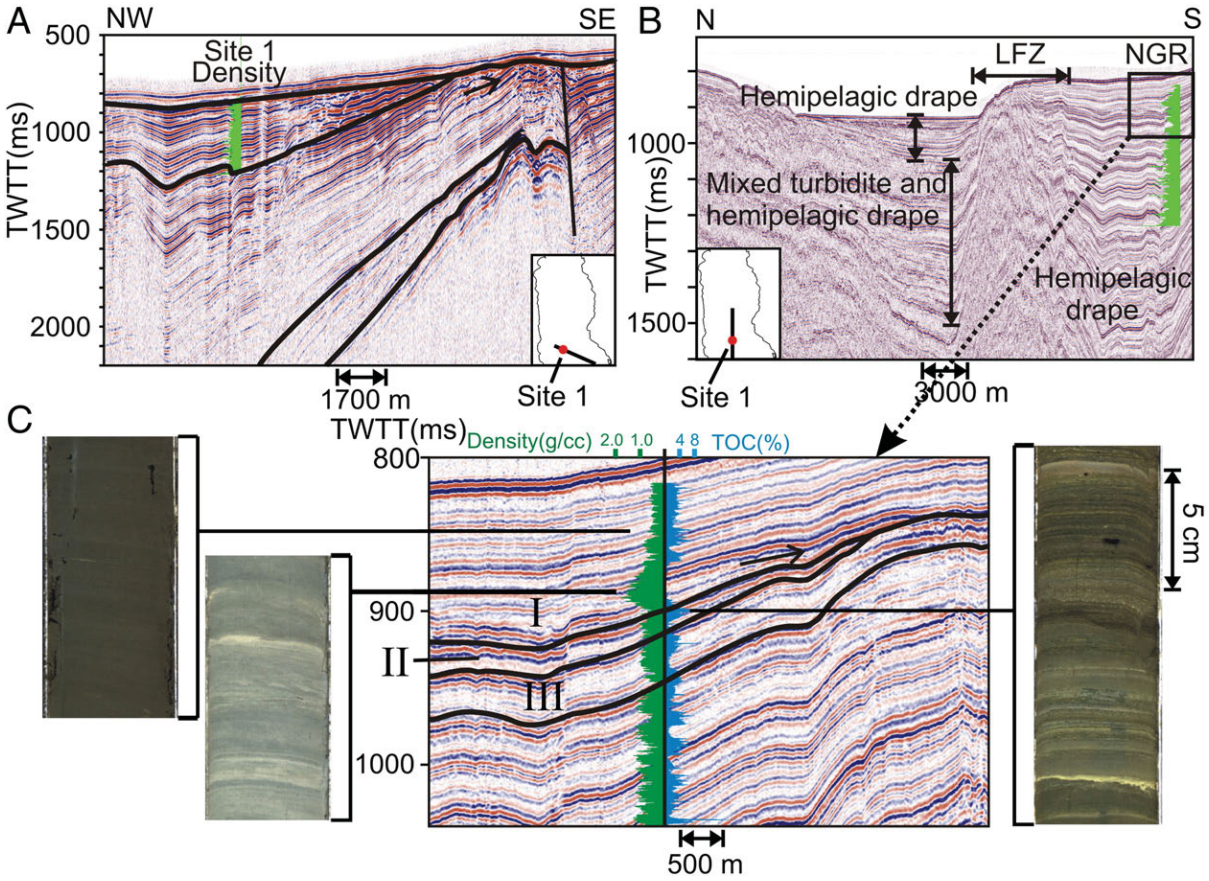

Fig. 9. (A) Deep basin-scale multichannel seismic-reflection profile 86-813 showing the subbottom extent of the core recovered at Drill Site 1, Natural Gamma-Ray (NGR) profile (increasing to the left) and the original PROBE sequence stratigraphy (Scholz et al., 1989). (B) High-resolution seismic profile showing Drill Site 1B with NGR increasing to the left. Note the Central Basin depocenter on the hanging wall of the LFZ where basin-fill facies are deposited. (C) Upper section of the seismic profile from (B) with Drill Site 1B density, TOC, sequence stratigraphy and associated digital imagery plotted. Note the erosional truncation at the base of Sequences I and II south of the drill site.

4.2.2. Central Basin Drill Site 1

The sedimentary fill at Drill Site 1 thickens to the northwest, as observed in multichannel seismic-reflection profiles (Fig. 9A) (Scholz et al., 1989; Flannery and Rosendahl, 1990). The base of Drill Site 1 is located at the sequence boundary between the second and third sequences out of the four observed in multichannel seismic-reflection data (Scholz et al., 1989; Flannery and Rosendahl, 1990). Seismic-reflection profiles at Drill Site 1 show primarily hemipelagic drape facies south of the LFZ (Fig. 9B). A high-resolution seismic-reflection profile at this site shows alternating high-amplitude and low-amplitude continuous reflections, several of which either onlap onto or are truncated by the basal bounding surfaces of Sequences I–III

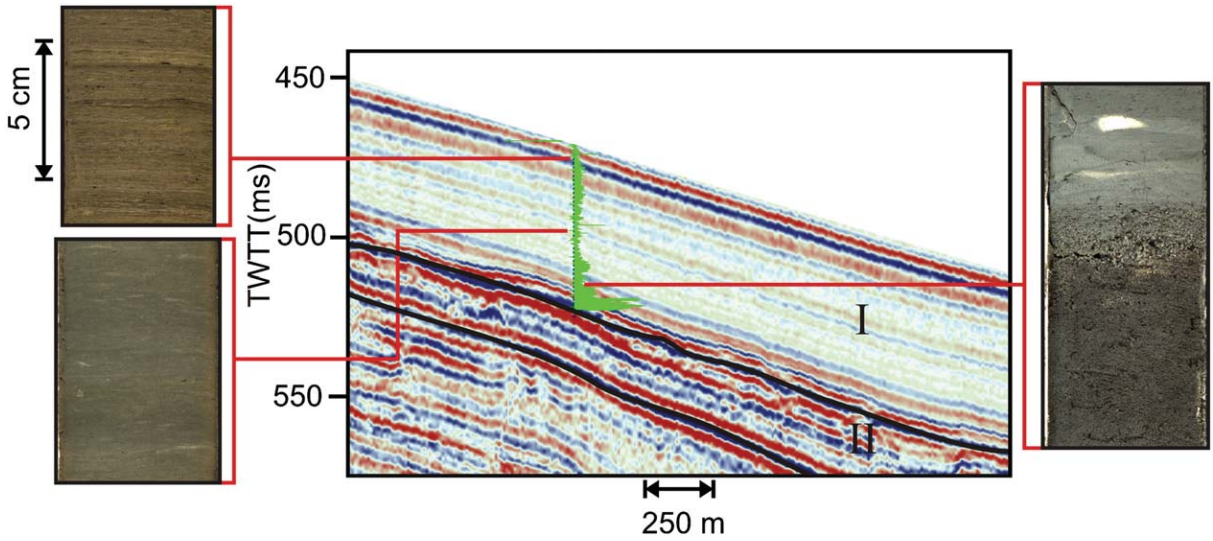

Fig. 10. Drill Site 2A in the N. Basin shows saturated bulk density (GRAPE — increasing to the right) superimposed on the seismic line with accompanying drill-core digital imagery and sequence stratigraphy.

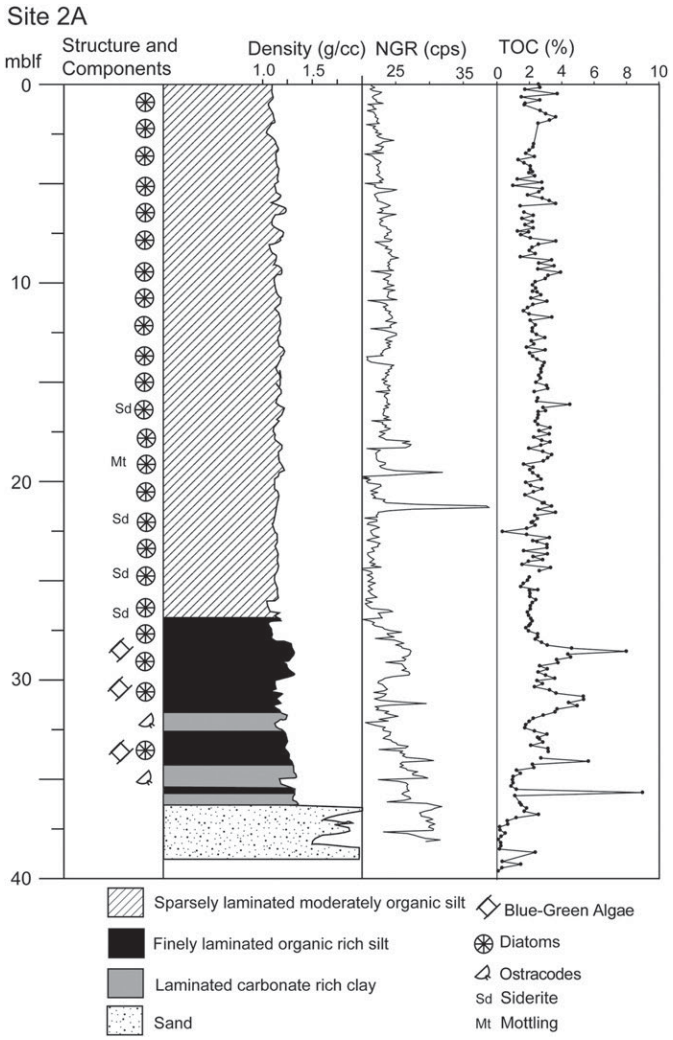

Fig. 11. Drill Site 2A stratigraphic column where lithofacies are initially identified. Total organic carbon (TOC), NGR, and density logs are plotted with sedimentary structures and compositional components.

(Fig. 9C). Each sequence thickens northward from their respective unconformities to the drill site. The sequences are correlated to Drill Site 1B TOC and GRAPE density curves and are plotted on the seismic-reflection profile (Fig. 9C). The basal bounding surface of each sequence is associated with light gray, carbonate- and ostracode-rich, organic-poor, high-density mud in the drill core, which is associated with a lowstand interval (Fig. 12). The base of Sequence I contains the thickest package of lowstand deposits, and is characterized by an interval of fine-grained sand with density values reaching 2.0 g/cm^3 and TOC values as low as 0.2%, suggesting an extended period of low lake stage (Figs. 9 and 12). The top of each sequence is associated with diatom-rich, organic-rich, laminated and non-laminated muds in the drill core, reflecting deposition during highstand intervals (Fig. 12). Each sequence defines one complete lake-level cycle, beginning with a lowstand event and followed by transgression and highstand conditions.

4.2.3. Seismic-amplitude response

Seismic–acoustic impedance is a function of density and velocity contrast (Best and Gunn, 1999). To validate the correlation between the drill-core data and the seismic-reflection data, synthetic seismograms were generated from whole-core density and sonic velocity logs from Drill Site 1B (Fig. 13). At the drill site, velocity varies by less than 10% down-core, however bulk density varies by a factor of two from 1.0 g/cm^3 to over 2.0 g/cm^3 over some intervals. This dependence of the impedance signal upon changes in density rather than sonic velocity is not uncommon in unlithified sediments (Brew and Mayer, 1998) and this is especially evident for the upper ~75 m of the section, where the sediments are least consolidated (Fig. 13). Six visual ties can be made between the synthetic seismogram and the trace data from the seismic-reflection profile across Drill Site 1. These ties are associated with sharp changes in density, located at ~846 ms, ~860 ms, ~870 ms, ~892 ms, ~902 ms, and ~918 ms (Fig. 13). The correlation coefficient between the seismic and synthetic traces is 0.49, because the frequency distribution of the drill-site data is different than that of the seismic-trace data (Latimer, 2005). However, the fact that the synthetic-trace data explains almost 50% of the variance of the seismic-trace data indicates that there is a statistical relationship between the two curves. Furthermore, amplitude spectra of the convolving wavelet and the seismic data appear to be similar in shape (Fig. 13B). The spectra of the drill-site reflection-coefficient series and the acoustic-impedance inversion reflectivity series are also similar in shape (Fig. 13C).

4.3. Age model applications

Scholz et al. (2007) make several visual ties between October 1–December 1 (start of the rainy season) mean insolation at 10° S and geochemical lake-level indicators from Drill Site 1, and note that intervals of low TOC, abundant ostracodes, and high Ca XRF counts

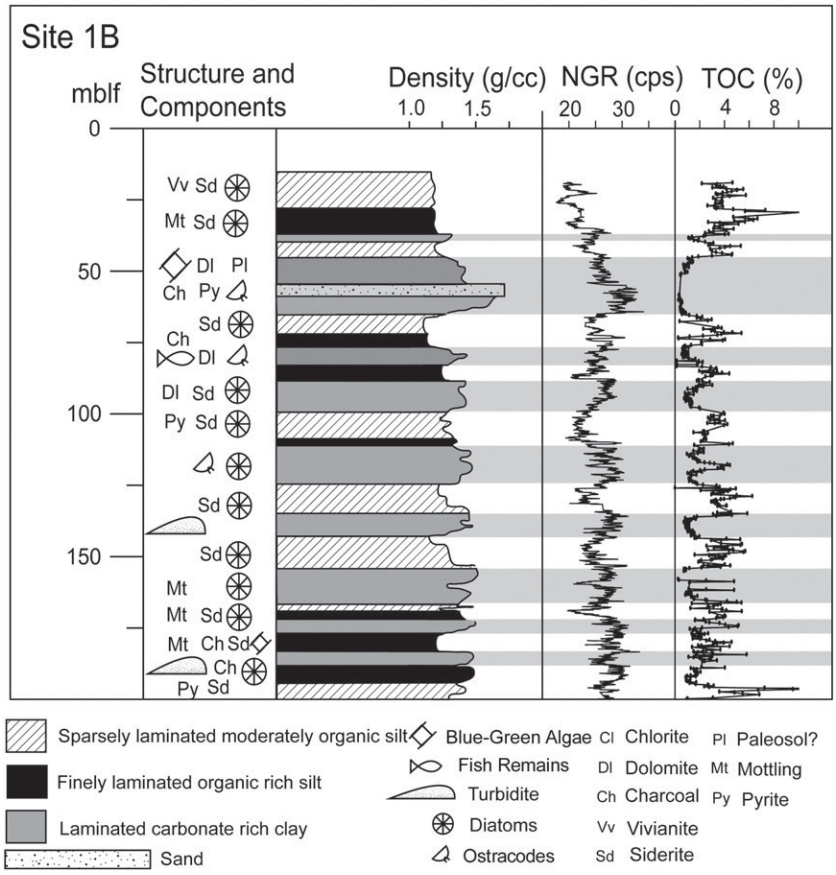

Fig. 12. Upper 200 m of the stratigraphic column of Drill Site 1B, with sedimentary structures, density, NGR (cps), and TOC (weight %). Lowstand lithofacies are highlighted in gray and are associated with highs in density and NGR and lows in TOC. Most of the organic-rich intervals are present immediately above interpreted lowstand events.

correlate to insolation minima. Using the age relationships determined for Drill Site 1 (Scholz et al., 2011-this issue), these intervals are correlated to sequence boundaries and lowstand seismic facies from the seismic-reflection data set (Fig. 14). We observe lowstands in both seismic-reflection data and drill core during the following time intervals: 62–65 ka (−200 m lowstand delta), 70–76 ka (−350 m lowstand delta), 85–110 ka (base of Sequence I), and 124–132 ka (base of Sequence II), and 148–156 ka (base of Sequence III) (Fig. 14). From 60 ka to the present, the water depths were very deep at this site. We observe evidence for increasing lake level from the −550 m lowstand at 85–110 ka to ~60 ka, punctuated by two lowstands of −350 m and −200 m, identified on seismic-reflection data from the North Basin as lowstand delta facies (Figs. 6 and 14).

5. Discussion

5.1. Sedimentation patterns and depositional environments

The river systems in the Lake Malawi catchment enter the lake at a variety of structural settings (Fig. 2). Therefore, stratigraphic evidence for lake-level variability is manifested slightly differently in each basin. However, we develop a conceptual model based on the several patterns that we observe in all basins that can be related to changes in seismic amplitude on seismic-reflection profiles and lithologic variability of the drill core. During highstands, coarse-grained sedimentation is concentrated in near-shore environments, while hemipelagic drape sediments are deposited throughout the rest of the basin (Fig. 15). When lake levels drop, runoff and sediment inputs are greatly limited because of arid conditions (Fig. 15). Cohen et al. (2007) and Beuning et al. (2011-this issue) describe severe aridity and semi-desert conditions in the Lake Malawi catchment during lake low-stands, with precipitation probably <400 mm/yr during these intervals. During transgressions, precipitation increases, increasing the runoff and sediment input, causing material stored on the landscape to be reworked and redistributed as dense coarse-grained sediment in the form of progradational deltas, turbidites, fans, and sublacustrine channels in the deeper parts of the basin (Fig. 4) (Perlmutter et al., 1995). These seismic facies have been observed throughout Lake Malawi within Sequence I (Fig. 4). This fundamental change in sedimentation patterns during lowstands results in changes in sediment density in the cores, and thus affects acoustic impedance in seismic-reflection profiles, causing highly variable amplitude responses in the seismic-reflection data (Fig. 9).

Organic-rich lithofacies are often observed following lowstand deposits (Figs. 11 and 12). During lowstands, areas previously covered by the lake are exposed, increasing the area available for terrigenous vegetation. During subsequent transgressions when sediment supply is high, increased runoff transports terrestrial organic matter into the lake basin, increasing nutrient availability, and fertilizing algal blooms. This is reflected in the drill core as high values of TOC, finely-laminated intervals which include layers rich in siliceous diatoms, and a distinctive green color from the digital imagery (Figs. 11 and 12). The diatom layers are also observed in XRF data as highs in silicon immediately following lowstands (Brown, 2011-this issue; Johnson et al., 2011-this issue).

The slope of the foresets of each clinoform package also increases during transgressions and during higher lake phases (Fig. 8). Orton and Reading (1993) have suggested that this relationship may be due to variability in the grain size of the deltas; the finer the dominant grain size, the lower the depositional slope. This suggests an increasing average grain size from the −500 m lowstand delta deposit to the −200 m lowstand delta deposits. This relationship may be due in part to the increased distance that sediment is transported

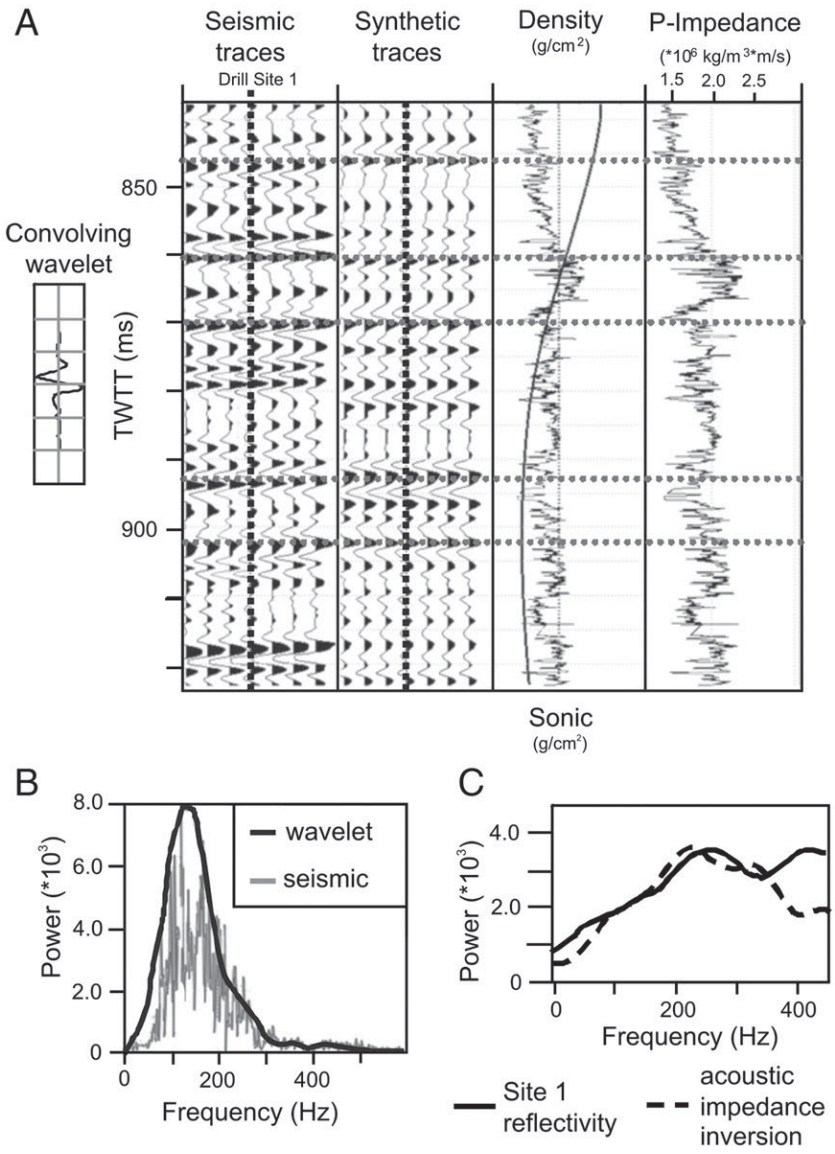

Fig. 13. (A) Synthetic seismogram plot of the upper ~75 m of Drill Site 1. Plotted from left to right are the convolving wavelet generated using Jason's wavelet estimation software, the seismic-trace data of 7 traces around Drill Site 1, the synthetic traces generated by Jason™, density (thin curve) and sonic logs (thick curve) at Drill Site 1, and acoustic-impedance log generated from the sonic and velocity logs. Interpreted crossing points are marked between the synthetic seismogram and the traces from the seismic-reflection profile. (B) Amplitude spectra of the convolving wavelet (black line) and the seismic-trace data (gray line). Note how the wavelet spectrum matches the shape and power of the seismic data in the frequency domain. (C) Amplitude spectra of the Drill Site 1 reflection coefficient series (solid line) and the resultant acoustic-impedance reflectivity series from inversion of the seismic-trace data using the estimated convolving wavelet and drill-site data as guides. Note that the two curves generally are similar in shape and power up to ~325 Hz. This relationship breaks down at frequencies greater than ~350 Hz, which may be due to noise in the seismic data. The correlation coefficient between the synthetic and seismic traces is 0.49. See text for further details on methodology and correlation coefficient discussion.

during the most severe low lake stages. Other environmental factors that may have impacted clinoform foreset slopes include changes in lake water salinity through periods of rising lake level, decreasing background depositional slope with increasing lowstand magnitude, and variations in sediment supply during arid versus wet climate phases. Regardless of the exact mechanism, this relationship is due to variations in the hydrologic system, which in this case, is ultimately linked to changing P–E conditions within the basin.

5.2. Lake-level chronology and implications

The sequence boundaries described in this paper define exposure surfaces when lake level was more than 550 m BPLL (Figs. 6, 7 and 9). These results are consistent with lake-level estimations from Scholz et al. (2007) and Cohen et al. (2007). On seismic-reflection profiles, we observe ancient delta deposits within Sequence I at various depths below modern lake level (Fig. 6). These can be interpreted in two ways: stillstands during long-term transgression or relative lowstands punctuating long-term transgression. Without drill-core data, it would be difficult to determine which interpretation is accurate. However, in Sequence I the drill-core data from site 1 suggests the former scenario for both the −200 m and −350 m deltas (Cohen et al., 2007; Scholz et al., 2007) (Figs. 9, 12, 14). Therefore, Sequence I could be divided into three subsequences, but for the purposes of this study, we interpret it as a single sequence. The absence of multiple delta deposits in Sequences II and III is probably due to later erosion.

Hypsometry generated from the water-bottom reflections on the seismic-reflection profiles shows that a low lake stage of 550 m represents a 97% volume reduction relative to modern conditions and an 89% reduction in surface area. Assuming subsidence rate equal to

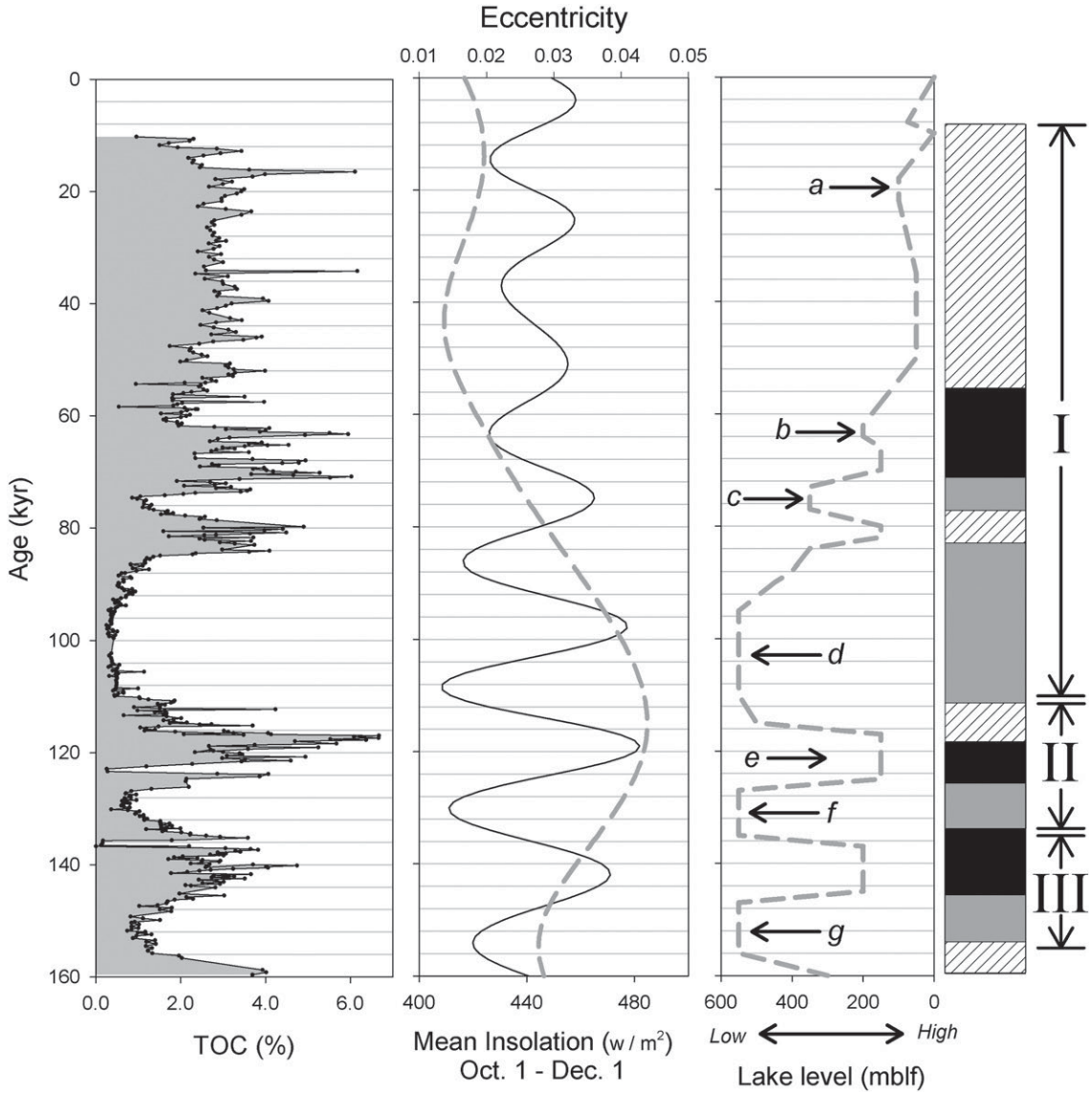

Fig. 14. Drill Site 1 composite 1B–1C TOC data plotted with mean insolation from October 1 to December 1 and eccentricity, an interpreted lake-level curve (Scholz et al., 2007), and lithostratigraphy from the drill core and sequence boundaries from the seismic-reflection data. In general, low TOC values correspond to insolation minima, Lake Malawi lowstands and sequence boundaries. Annotated lowstand events (a–f) are interpreted as follows: (a) The Last Glacial Maximum (LGM) that has been interpreted previously as a Lake Malawi ~ −100 m lowstand event (e.g. Johnson et al., 2002). We suggest that an observed −75 m lowstand delta offshore the Dwangwa River may be associated with this event (Fig. 4). (b) The −200 m lowstand event associated with lowstand deltas throughout the lake (Figs. 4 and 6). (c) The −350 m lowstand event associated with lowstand deltas observed in the North Basin (Figs. 4 and 6). (d) Prolonged lowstand associated with the −500 m (Figs. 4 and 6) lowstand deltas observed in the North Basin and with a −550 m erosional truncation surface south of Drill Site 1 (Fig. 9). (e) A relative highstand delta observed within Sequence II at −300 m, which constrains the minimum magnitude of the highstand to 300 m BPLL within the sequence. (f) A lowstand associated with the −500 m (Figs. 4 and 6) lowstand delta observed in the North Basin and with a −550 m erosional truncation surface south of Drill Site 1 (Fig. 9). (g) A lowstand event associated with the base of Sequence III (Fig. 6).

sedimentation rate, a 550 m BPLL low lake stand would result in desiccation of the North Basin, which has a maximum water depth of ~500 m (Fig. 4). However, due to the bathymetric high associated with the accommodation zone between the North and Central Basins, a lake-level drop of ~465 m or greater would hydrologically isolate the two basins (Fig. 1). This may have allowed the North Basin to persist as a ~50 m deep, ~50 km long lake, during severe arid intervals. When the two basins are isolated their respective water balances will be different, and each will respond uniquely to atmospheric changes. It is possible the timing of the North Basin −500 m lowstand delta was coincident with the −550 m erosional truncation observed in the Central Basin at the base of Sequence I and II.

Deltaic deposits associated with the −200 m low lake stage during the most recent transgression are observed extensively in the seismic-reflection data (Fig. 4), and are the largest, best preserved, and most prevalent paleodeltas observed along the full length of the lake. Buoniconti (2000) and Martin (1997) estimated this event at ~70 ka simply by extrapolating sedimentation rates from shallow cores. This is in general agreement with the drill-core interpretation of this lowstand, which extended from 65–60 ka (Scholz et al., 2007). Scholz et al. (2007) describe lake-level change in Lake Malawi as a consequence of eccentricity-modulated precessional forcing prior to 60 ka. During intervals of high eccentricity (i.e. 160–60 ka), precession cycles associated with insolation dominate tropical African climate (Fig. 14), inducing severe low lake stages every ~11 ka and ~23 ka. When eccentricity is low (i.e. 70 ka to present), lake level stabilizes and relative highstand conditions persist (Fig. 14). These trends are manifested in seismic-reflection profiles as lowstand facies observed throughout Lake Malawi from 160 ka to 60 ka and highstand facies over the last 60 ka.

It is possible that the ancient delta clinoforms observed offshore of the Dwangwa River system at ~75 m and ~100 m are associated with

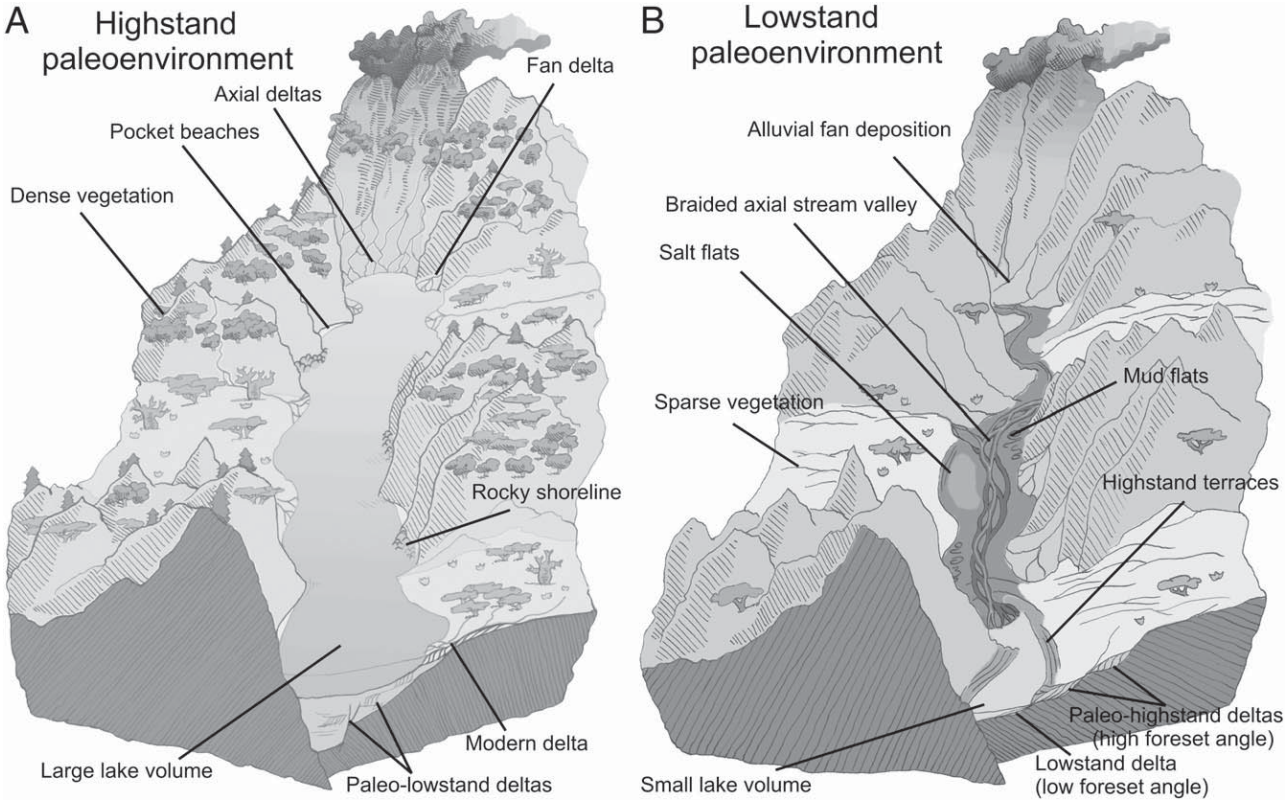

Fig. 15. (A, B) Paleoenvironmental conceptual models of a rift lake basin in highstand and lowstand states, with key features of each environment labeled. Modern Lake Malawi is an example of the highstand environmental system. The severe lowstands documented in this paper are an analog for the lowstand paleoenvironment model.

a relatively minor Last Glacial Maximum (LGM) lowstand (Fig. 4). It is well documented that the LGM was a dry period throughout much of East Africa (e.g. Johnson et al., 1996; Barker and Gasse, 2003; Felton et al., 2007). In Lake Malawi coarse-grained seismic facies are not observed deep in the basin during these intervals, suggesting the LGM was a minor event relative to the earlier severe lowstands and subsequent transgressions (Sequences I–III). The lowstand deltas of the Dwangwa system suggest that LGM lake levels were between 75 m and 100 m BPLL.

6. Conclusions

(1) Seismic-reflection data from Lake Malawi reveal evidence for extreme low lake stages, manifested as coarse-grained seismic facies, such as lowstand deltas, fans, turbidites, and sublacustrine channels in as much as 500 m modern water depth. Erosional truncation surfaces in the Central Basin are in as much as 550 m modern water depth.

(2) We identify three sequences (I–III) in the North Basin and interpret them throughout the lake. Each sequence represents a complete lake-level cycle, where a basal bounding surface representing a very severe (more than 200 m lake-level drop) lowstand is overlain by transgressive and highstand facies.

(3) The seismic stratigraphic framework is linked to each drill site, where lowstand lithofacies are correlated to sequence boundaries. Lowstands are associated with organic carbon values as low as 0.2–2%, and densities as high as 2.0 g/cm^3. Drill-core and seismic correlations suggest lowstands lower than 550 m below present lake level during the past ~160 ka. These lake-level drops resulted in a 97% volume reduction and an 89% of surface area reduction relative to modern conditions. Subsequent transgressions are associated with increased sediment supply due to increased runoff, increasing the organic matter flux into the basin, as well as with the transport of coarse-grained sediment into the deeper parts of the basin.

(4) Several visual ties can be made between synthetic seismogram data from Drill Site 1 and seismic-trace data at the drill site, where the cross correlation between the two data sets is 0.49. Density rather than sonic velocity is the primary control on seismic amplitude in the upper ~75 m of section at the drill site.

(5) Water levels in Lake Malawi dropped to 75–100 m below modern levels during the Last Glacial Maximum, but this somewhat arid interval was a relatively minor event compared to severe lowstands that developed during the megadroughts that occurred between 160 and 60 ka.

Acknowledgements

General contracting and barge modifications during drilling operations were carried out by the University of Rhode Island and Lengeek Vessel Engineering, Inc. We thank ADPS Ltd. and Seacore Ltd. for marine operations and drilling support, respectively, on the Viphya drilling vessel. DOSECC, Inc., the Geological Survey of Malawi, Malawi Department of Surveys, and Malawi Lake Services provided technical and logistical support. Drill-core processing and analysis were performed at the National Lake Core Repository at the University of Minnesota. Support for seismic data acquisition was provided by the Lacustrine Rift Basin Industrial Associates of Syracuse University. Landmark Graphics Corporation provided seismic data processing and interpretation software, P. K. Cattaneo provided assistance with seismic-reflection data acquisition and processing, and R. Latimer assisted with synthetic seismogram generation. Funding for scientific drilling on Lake Malawi was provided by the U.S. National Science Foundation and by the International Continental Scientific Drilling Program. Scientific analysis of drill-core samples has been supported

by the U.S. National Science Foundation. We thank the government of Malawi for permission to conduct this research. S. Colman, an anonymous reviewer, journal editor F. Kop, and M. McGlue provided helpful reviews and comments that greatly improved the manuscript.

References

Aksu, A.E., Ulug, A., Piper, D.J.W., Konuk, Y.T., Turgut, S., 1992. Quaternary sedimentary history of Adana, Cilicia and Iskenderun Basins, northeast Mediterranean Sea. Marine Geology 104, 55–71.

Back, S., De Batist, M., Strecker, M.R., Vanhauwaert, P., 1999. Quaternary depositional systems in northern Lake Baikal, Siberia. The Journal of Geology 107, 1–12.

Barker, P., Gasse, F., 2003. New evidence for a reduced water balance in East Africa during the Last Glacial Maximum: implication for model-data comparison. Quaternary Science Reviews 22 (8–9), 823–837.

Best, A.I., Gunn, D.E., 1999. Calibration of marine sediment core loggers for quantitative acoustic impedance studies. Marine Geology 160 (1–2), 137–146.

Beuning, K.R.M., Zimmerman, K.A., Ivory, S.J., Cohen, A.S., 2011. Vegetation response to glacial–interglacial climate variability near Lake Malawi in the southern African tropics. Palaeogeography, Palaeoclimatology, Palaeoecology 303, 81–92 (this issue).

Brew, D.S., Mayer, L.A., 1998. Modeling of Pliocene–Pleistocene abyssal mudwaves using synthetic seismograms. Marine Geology 149, 3–16.

Broecker, W.S., Peteet, D.M., Hajdas, I., Lin, J., Clark, E., 1998. Antiphasing between rainfall in Africa's Rift Valley and North America's Great Basin. Quaternary Research 50 (1), 12–20.

Brown, E.T., 2011. Lake Malawi's response to "megadrought" terminations: Sedimentary records of flooding, weathering and erosion. Palaeogeography, Palaeoclimatology, Palaeoecology 303, 120–125 (this issue).

Brown, E.T., Johnson, T.C., 2005. Coherence between tropical East African and South American records of the Little Ice Age. Geochemistry, Geophysics, and Geosystems 6 (12) 11 pp.

Brown, E.T., Johnson, T.C., Scholz, C.A., Cohen, A.S., King, J.W., 2007. Abrupt change in tropical African climate linked to the bipolar seesaw over the past 55,000 years. Geophysical Research Letters 34 (L20702) 5 pp.

Buoniconti, M.R., 2000. The sequence stratigraphy of the Songwe delta, a rift lake axial margin delta, Lake Malawi, East Africa. Masters Thesis, University of Miami.

Burnett, A.P., Soreghan, M.J., Scholz, C.A., Brown, E.T., 2011. Tropical East African climate change and its relation to global climate: A record from Lake Tanganyika, Tropical East Africa, over the past 90+ kyr. Palaeogeography, Palaeoclimatology, Palaeoecology 303 (1–4), 155–167 (this issue).

Butch, J.L., 1996. Compositional and textural analysis of sandy sediments across two rift lake deltas: Songwe–Kiwira and Dwangwa deltas, Lake Malawi, East Africa. Masters Thesis, University of North Carolina at Chapel Hill.

Castañeda, I.S., Werne, J.P., Johnson, T.C., 2007. Wet and arid phases in the southeast African tropics since the Last Glacial Maximum. Geology 35 (9), 823–826.

Cathro, D.L., Austin Jr., J.A., Moss, G.D., 2003. Progradation along a deeply submerged Oligocene–Miocene heterozoan carbonate shelf: how sensitive are clinoforms to sea level variations? AAPG Bulletin 87 (10), 1547–1574.

Chorowicz, J., 2005. The East African Rift System. Journal of African Earth Sciences 43, 379–410.

Chu, D., Gordon, R.G., 1999. Evidence for motion between Nubia and Somalia along the southwest Indian ridge. Nature 298, 64–67.

Clemens, S., Prell, W., Murray, D., Shimmield, G., Weedon, G., 1991. Forcing mechanisms of the Indian Ocean monsoon. Nature 353 (24), 720–725.

Clement, A.C., Hall, A., Broccoli, A.J., 2004. The importance of precessional signal in the tropics. Climate Dynamics 22, 327–341.

Colman, S.M., Karabanov, E.B., Nelson III, C.H., 2003. Quaternary sedimentation and subsidence history of Lake Baikal, Siberia, based on seismic stratigraphy and coring. Journal of Sedimentary Research 73 (6), 941–956.

Cohen, A.S., Stone, J.R., Beuning, K.R.M., Park, L.E., Reinthal, P.N., Dettman, D., Scholz, C.A., Johnson, T.C., King, J.W., Talbot, M.R., Brown, E.T., Ivory, S.J., 2007. Ecological consequences of early Late Pleistocene megadroughts in tropical Africa. Proceedings of the National Academy of Sciences 104 (42), 16422–16427.

Crossley, R., Crow, M.J., 1980. The Malawi rift. In: Carelli, A. (Ed.), Geodynamic Evolution of the Afro–Arabian Rift System. Accademia Nazionale dei Lincei, Rome, Italy, pp. 78–87.

deMenocal, P.B., 1995. Plio–Pleistocene African climate. Science 270, 53–59.

Driscoll, N.W., Karner, G.D., 1999. Three-dimensional quantitative modeling of clinoform development. Marine Geology 154, 383–398.

Ebinger, C.J., 1989. Tectonic development of the western branch of the East African rift system. Geological Society of America Bulletin 101, 885–903.

Einsele, G., 2000. Sedimentary Basins; Evolution, Facies, and Sediment Budget. Springer, Berlin.

Felton, A.A., Russell, J.M., Cohen, A.S., Baker, M.E., Chesley, J.T., Lezzar, K.E., McGlue, M.M., Pigati, J.S., Quade, J., Stager, J.C., Tiercelin, J.J., 2007. Paleolimnological evidence for the onset and termination of glacial aridity from Lake Tanganyika, Tropical East Africa. Palaeogeography, Palaeoclimatology, Palaeoecology 252, 405–423.

Filippi, M.L., Talbot, M.R., 2005. The paleolimnology of northern Lake Malawi over the last 25 ka based upon the elemental and stable isotopic composition of sedimentary organic matter. Quaternary Science Reviews 24, 1303–1328.

Finney, B.P., Johnson, T.C., 1991. Sedimentation in Lake Malawi (East Africa) during the past 10,000 years; a continuous paleoclimatic record from the southern tropics. Palaeogeography, Palaeoclimatology, Palaeoecology 85 (3–4), 351–366.

Finney, B.P., Scholz, C.A., Johnson, T.C., Trumbore, S., 1996. Late Quaternary lake-level changes of Lake Malawi. In: Johnson, T.C., Odada, E.O. (Eds.), The Limnology, Climatology, and Paleoclimatology of the East African Lakes. Gordon and Breach, Amsterdam, pp. 495–508.

Flannery, J.W., 1988. The acoustic stratigraphy of Lake Malawi, East Africa. Masters Thesis, Duke University.

Flannery, J.W., Rosendahl, B.R., 1990. The seismic stratigraphy of Lake Malawi, Africa; implications for interpreting geological processes in lacustrine rifts. Journal of African Earth Sciences 10 (3), 519–548.

Fritz, S.C., Baker, P.A., Lowenstein, T.K., Seltzer, G.O., Rigsby, C.A., Dwyer, G.S., Tapia, P.M., Arnold, K.K., Ku, T., Luo, S., 2004. Hydrologic variation during the last 170,000 years in the southern hemisphere tropics of South America. Quaternary Research 61, 95–104.

Fulthorpe, C.S., Austin Jr., J.A., 2008. Assessing the significance of along-strike variations of middle to late Miocene prograding clinoformal sequence geometries beneath the New Jersey continental shelf. Basin Research 20 (2), 269–283.

Gasse, F., Ledee, V., Massault, M., Fontes, J., 1989. Water-level fluctuations of Lake Tanganyika in phase with oceanic changes during the last glaciation and deglaciation. Nature 342, 57–59.

Hooghiemstra, H., Melice, J.L., Berger, A., Shackleton, N.J., 1993. Frequency spectra and paleoclimatic variability of the high-resolution 30–1450 ka Funza I pollen record (Eastern Cordillera, Colombia). Quaternary Science Reviews 12 (2), 141–156.

Johnson, T.C., Ng'ang'a, P., 1990. Reflections on a rift lake. In: Katz, B.J. (Ed.), Lacustrine Basin Exploration: Case Studies and Modern Analogs. . AAPG. Memoir, vol. 50. Tulsa, pp. 113–135.

Johnson, T.C., Scholz, C.A., Talbot, M.R., Kelts, K., Ricketts, R.D., Ngobi, G., Beuning, K., Ssemmanda, I., McGill, J.W., 1996. Late Pleistocene desiccation of Lake Victoria and Rapid Evolution of Cichlid Fishes. Science 273, 1091–1093.

Johnson, T.C., Brown, E.T., McManus, J., Barry, S., Barker, P., Gasse, F., 2002. A high-resolution paleoclimate record spanning the past 25,000 years in southern East Africa. Science 296, 113–114, 131–132.

Johnson, T.C., Brown, E.T., Shi, J., 2011. Biogenic silica deposition in Lake Malawi, East Africa over the past 150,000 years. Palaeogeography, Palaeoclimatology, Palaeoecology 303, 103–109 (this issue).

Kidd, C.H.R., 1983. A water resources evaluation of Lake Malawi and the Shire River. UNDP Project MLW/77/012. World Meteorological Organization, Geneva.

Kingdon, M.J., Bootsma, H.A., Mwita, J., Mwichande, B., Hecky, R.E., 1999. River discharge and water quality. In: Bootsma, H.A., Hecky, R.E. (Eds.), Water Quality Report. Lake Malawi/Nyasa Biodiversity Conservation Project, Malawi, pp. 29–69.

Latimer, R., 2005. Uses, Abuses, and Examples of Seismic-Derived Acoustic Impedance Data: What Does the Interpreter Need to Know? SEG/AAPG Distinguished Lecture Program. http://www.seg.org/SEGportalWEBproject/portals/SEG_Online.portal?_nfpb=true&_pageLabel=pg_gen_content&Doc_Url=prod/SEG-Education/Ed-Distinguish-Lect-Program/fall2005/latimerabstract.htm.

Lezzar, K.E., Tiercelin, J.-J., De Batist, M., Cohen, A.S., Bandora, T., Van Rensbergen, P., Le Turdu, C., Mifundu, W., Klerkx, J., 1996. New seismic stratigraphy and Late Tertiary history of the North Tanganyika Basin, East African Rift system, deduced from multichannel and high-resolution reflection seismic data and piston core evidence. Basin Research 8, 1–28.

Malawi Department of Surveys, 1983. National Atlas of Malawi: Blantyre, Malawi. 79 pgs.

Martin, M.R., 1997. The sequence stratigraphy of a rift lake flexural margin delta: Dwangwa delta, Lake Malawi, East Africa. Masters Thesis, University of Houston.

Metzger, J.M., Flemings, P.B., Christie-Blick, N., Mountain, G.S., Austin Jr., J.A., Hesselbo, S.P., 2000. Late Miocene to Pleistocene sequences at the New Jersey outer continental shelf (ODP leg 174A, sites 1071 and 1072). Sedimentary Geology 134, 149–180.

McGlue, M.M., Scholz, C.A., Karp, T., Ongodia, B., Lezzar, K.E., 2006. Facies architecture of flexural margin lowstand delta deposits in Lake Edward, East African Rift: constraints from seismic reflection imaging. Journal of Sedimentary Research 76, 942–958.

Monteverde, D.H., Mountain, G.S., Miller, K.G., 2008. Early Miocene sequence development across the New Jersey margin. Basin Research, 20 (2), 249–267.

Morley, C.K., 1999. How successful are analogue models in addressing the influence of pre-existing fabrics on rift structure? Journal of Structural Geology 21, 1267–1274.

Morley, C.K., Nelson, R.A., Patton, T.L., Munn, S.G., 1990. Transfer zones in the East African Rift system and their relevance to hydrocarbon exploration in rifts. AAPG Bulletin 74 (8), 1234–1253.

Nyblade, A.A., Brazier, R.A., 2002. Precambrian lithospheric controls on the development of the East African rift system. Geology 30, 755–758.

Olsen, P.E., Kent, D.V., 1996. Milankovitch climate forcing in the tropics of Pangaea during the Late Triassic. Palaeogeography, Palaeoclimatology, Palaeoecology 122 (1–4), 1–26.

Orton, G.J., Reading, H.G., 1993. Variability of deltaic processes in terms of sediment supply, with particular emphasis on grain size. Sedimentology 40, 475–512.

Owen, R.B., Crossley, R., Johnson, T.C., Tweddle, D., Kornfield, I., Davison, S., Eccles, D.H., Engstrom, D.E., 1990. Major low lake levels of Lake Malawi and their implications for speciation rates in cichlid fishes. Proceedings of the Royal Society of London. Series B, Biological Sciences B240, 519–553.

Partridge, T.C., DeMenocal, P.B., Lorentz, S.A., Paiker, M.J., Vogel, J.C., 1997. Orbital forcing of climate over South Africa: a 200,000-year rainfall record from the Pretoria Saltpan. Quaternary Science Reviews 16, 1125–1133.

Perlmutter, M.A., Brennan, P.A., Hook, S.C., Dempster, K., Pasta, D., 1995. Global cyclostratigraphic analysis for the Seychelles Southern Shelf for potential reservoir, seal and source rocks. Sedimentary Geology 96, 93–118.

Pilskaln, C.H., Johnson, T.C., 1991. Seasonal signals in Lake Malawi sediments. Limnology and Oceanography 36 (3), 544–557.

Pokras, E.M., Mix, A.C., 1987. Earth's precession cycle and Quaternary climate change in tropical Africa. Nature 326, 486–487.

Powers, L.A., Johnson, T.C., Werne, J.P., Castaneda, I.S., Hopmans, E.C., Sinninghe Damste, J.S., Schouten, S., 2005. Large temperature variability in the southern African tropics since the last glacial maximum. Geophysical Research Letters 32 (8) 4 pgs.

Reynolds, D.J., Steckler, M.S., Coakley, B.J., 1991. The role of the sediment load in sequence stratigraphy; the influence of flexural isostasy and compaction. Journal of Geophysical Research 96 (B4), 6931–6949.

Ring, U., 1994. The influence of pre-existing structure on the evolution of the Cenozoic Malawi Rift (East African Rift System). Tectonics 13, 313–326.

Rosendahl, B.R., 1987. Architecture of continental rifts with special reference to East Africa. Annual Review of Earth and Planetary Sciences 15, 445–503.

Russell, J.M., Johnson, T.C., 2007. Little Ice Age drought in equatorial Africa: Intertropical Convergence Zone migration and El Niño–Southern Oscillation variability. Geology 35 (1), 21–24.

Saller, A.H., Noah, J.T., Ruzuar, A.P., Schneider, R., 2004. Linked lowstand delta to basin-floor fan deposition, offshore Indonesia; an analog for deep-water reservoir systems. AAPG Bulletin 88 (1), 21–46.

Schlische, R.W., 1995. Geometry and origin of fault-related folds in extensional settings. AAPG Bulletin 79 (11), 1661–1678.

Scholz, C.A., 1995a. Seismic stratigraphy of an accommodation-zone margin rift-lake delta, Lake Malawi, Africa. Geological Society Special Publications 80, 183–195.

Scholz, C.A. (Ed.), 1995b. Lake Malawi Sublacustrine Fan Study — Fan Study Seismic Atlas: University of Miami Rosenstiel School of Marine and Atmospheric Science, Miami, Florida.

Scholz, C.A., 1995c. Deltas of the Lake Malawi Rift, East Africa: seismic expression and exploration implications. AAPG Bulletin 79 (11), 1679–1697.

Scholz, C.A., 2001. Applications of seismic sequence stratigraphy in lacustrine basins. In: Last, W.M., Smol, J.P. (Eds.), Tracking Environmental Change Using Lake Sediments. Basin Analysis, Coring and Chronological Techniques, vol. 1. Springer, Berlin, pp. 7–22.

Scholz, C.A., Rosendahl, B.R., 1988. Low lake stages in Lakes Malawi and Tanganyika, East Africa, delineated with multifold seismic data. Science 240, 1645–1648.

Scholz, C.A., Rosendahl, B.R., Versfelt, J.W., Flannery, J., Ng'ang'a, P., Scott, D., Specht, T., 1989. Seismic Atlas of Lake Malawi (Nyasa), East Africa. Published by Project PROBE, Duke University.

Scholz, C.A., Rosendahl, B.R., Scott, D.L., 1990. Development of coarse-grained facies in lacustrine rift basins; examples from East Africa. Geology 18 (2), 140–144.

Scholz, C.A., Johnson, T.C., McGill, J.W., 1993. Deltaic sedimentation in a rift valley lake; new seismic reflection data from Lake Malawi (Nyasa), East Africa. Geology 21 (5), 395–398.

Scholz, C.A., King, J.W., Ellis, G.S., Swart, P.K., Stager, J.C., Colman, S.M., 2003. Paleolimnology of Lake Tanganyika, East Africa, over the past 100 kyr. Journal of Paleolimnology 30, 139–150.

Scholz, C.A., Cohen, A.S., Johnson, T.C., King, J.W., Moran, K., 2006. The 2005 Lake Malawi Drilling Project. Scientific Drilling 2, 17–19.

Scholz, C.A., Johnson, T.C., Cohen, A.C., King, J.W., Peck, J.A., Overpeck, J.T., Talbot, M.R., Brown, E.T., Kalindekafe, L., Amoako, P.Y.O., Lyons, R.P., Shanahan, T.M., Castaneda, I.S., Heil, C.W., Forman, S.L., McHargue, L.R., Beuning, K.R., Gomez, J., Pierson, J., 2007. East African megadroughts between 135 and 75 thousand years ago and bearing on early-modern human origins. Proceedings of the National Academy of Sciences 104 (42), 16416–16421.

Scholz, C.A., Talbot, M.R., Brown, E.T., Lyons, R.P., 2011. Lithostratigraphy, physical properties and organic matter variability in Lake Malawi Drillcore sediments over the past 145,000 years. Palaeogeography, Palaeoclimatology, Palaeoecology 303, 38–50 (this issue).

Soreghan, M.J., Scholz, C.A., Wells, J.T., 1999. Coarse-grained, deep-water sedimentation along a border fault margin of Lake Malawi, Africa: seismic stratigraphic analysis. Journal of Sedimentary Research 69 (4), 832–846.

Specht, T.D., Rosendahl, B.R., 1989. Architecture of the Lake Malawi Rift, East Africa. In: Rogers, J.J.W., Rach, N.M. (Eds.), Journal of African Earth Sciences Special Issue. Africa Rifting, vol. 8. Elsevier, London, pp. 355–382.

Spigel, R.H., Coulter, G.W., 1996. Comparison of hydrology and physical limnology of the East African Great Lakes: Tanganyika, Malawi, Victoria, Kivu and Turkana (with reference to some North American Great Lakes). In: Johnson, T.C., Odada, E. (Eds.), The Limnology, Climatology and Paleoclimatology of the East African lakes. Gordon and Breach, Amsterdam, pp. 103–140.

Trauth, M.H., Deino, A.L., Strecker, M.R., 2001. Response of the East African climate to orbital forcing during the last interglacial (130–117 ka) and the early last glacial (117–60 ka). Geology 29 (6), 499–502.

Trauth, M.H., Deino, A.L., Bergner, A.G.N., Strecker, M.R., 2003. East African climate change and orbital forcing during the last 175 kyr BP. Earth and Planetary Science Letters 206 (3–4), 297–313.

Trauth, M.H., Maslin, M.A., Deino, A.L., Strecker, M.R., 2005. Late Cenozoic moisture history of East Africa. Science 209, 2051–2053.

Vail, P.R., Mitchum Jr., R.M., Todd, R.G., Widmier, J.M., Thompson III, S., Sangree, J.B., Bubb, J.N., Hatlelid, W.G., 1977. Seismic stratigraphy and global changes of sea level. In: Clayton, C.E. (Ed.), Seismic Stratigraphy — Applications to Hydrocarbon Exploration. AAPG Mem., vol. 26, pp. 49–212.

Versfelt, J., Rosendahl, B.R., 1989. Relationships between pre-rift structure and rift architecture in Lakes Tanganyika and Malawi, East Africa. Nature 337 (26), 354–357.

Vollmer, M.K., Bootsma, H.A., Hecky, R.E., Patterson, G., Halfman, J.D., Edmond, J.M., Eccles, D.H., Weiss, R.F., 2005. Deep-water warming trend in Lake Malawi, East Africa. Limnology and Oceanography 50 (2), 727–732.

Wells, J.T., Scholz, C.A., Soreghan, M.J., 1999. Processes of sedimentation on a lacustrine border-fault margin; interpretation of cores from Lake Malawi, East Africa. Journal of Sedimentary Research 69 (4), 816–831.

Williams, D.F., Peck, J., Karabanov, E.B., Prokopenko, A.A., Kravchinsky, V., King, J., Kuzmin, M.I., 1997. Lake Baikal record of continental climate response to orbital insolation during the past 5 million years. Science 278, 1114–1117.

Wright, C., Kgaswane, E.M., Kwadiba, M.T.O., Simon, R.E., Nguuri, T.K., McRae-Samuel, R., 2003. South African seismicity, April 1997 to April 1999, and regional variations in the crust and uppermost mantle of the Kaapvaal craton. Lithos 71, 369–392.

Xie, X., Müller, R.D., Ren, J., Jiang, T., Zhang, C., 2008. Stratigraphic architecture and evolution of the continental slope system in offshore Hainan, northern South China Sea. Marine Geology 247, 129–144.

Yirgu, G., Ebinger, C.J., Maguire, P.K.H., 2006. The Afar volcanic province within the East African Rift System: introduction. Geological Society of London Special Publications 259, 1–6.